JOURNAL OF GEOPHYSICAL RESEARCH, VOL. 104, NO. C12, PAGES 29,637–29,661, DECEMBER 15, 1999

An analysis of tropical instability waves in a numerical model of the Pacific Ocean
2. Generation and energetics of the waves

S. Masina,[1] S.G.H. Philander, and A.B.G. Bush[2]

Atmospheric and Oceanic Sciences Program, Princeton University, Princeton, New Jersey

Abstract. The instability processes which generate unstable waves with characteristics similar to observed tropical instability waves in the Pacific Ocean are examined through a local energy analysis based on deviations from the time mean flow. Numerical experiments indicate that the waves develop preferentially in the eastern Pacific along the northern temperature front and have a westward phase speed and a structure with two peaks in amplitude: one located on the equator and the other a few degrees north of it. The energy analysis shows that the "two-peak" structure of the eastern waves is explained by two different instability processes which occur at different latitudes. In the time mean sense the region north of the equator is baroclinically unstable, while barotropic instability prevails at the equator. The life cycle of the waves is revealed by the time evolution of the energetics. Baroclinic instability is the dominant triggering mechanism which induces growth of the waves along the northern temperature front. The eddy pressure fluxes radiate energy south of the equator where the meridional shear between the Equatorial Undercurrent and the South Equatorial Current becomes barotropically unstable. From the numerical simulations, there is evidence of a second unstable region in the central Pacific south of the equator where the instabilities have a lower phase speed. The energy analysis also shows that these waves grow from both barotropic and baroclinic conversions.

1. Introduction

To date, one of the most interesting unresolved issues related to the tropical instability waves (TIWs) concerns the instability processes which generate the waves and the energetics involved during their growth. Some data analyses suggest that TIWs arise from an instability of the mean flow, primarily through the barotropic shear between the EUC and the SEC north of the equator [*Qiao and Weisberg,* 1995]. However, other analyses demonstrate a significant conversion of mean potential energy to eddy energy through baroclinic conversion [*Hansen and Paul,* 1984; *Wilson and Leetmaa,* 1988]. Most of the data suggest that both barotropic and baroclinic conversions are occurring, but whether or not they occur at the same time in the same location is an important question that has not been answered yet.

The hypothesis of two decoupled instabilities [*Flament et al.,* 1996], one occurring just north of the equator and the second at the equatorial front between 3°N and 6°N, has been supported by an energy analysis [*Luther and Johnson,* 1990] that shows a large mean flow to eddy kinetic energy conversion in the former region and a large mean flow to eddy potential energy conversion in the latter region. The energy analysis by *Luther and Johnson* [1990] shows that the two different types of instabilities arise at different times during the year and that the potential energy production at the equatorial front ($\simeq$ 6°N), which is at maximum during the winter, is not temporally correlated with the barotropic conversion occurring a few degrees south of it during the boreal summer and fall. The hypothesis that the instability growing near 6°N is excited by the shear between the South Equatorial Current (SEC) and North Equatorial Countercurrent (NECC) [*Flament et al.,* 1996] has not been supported by any evidence of significant Reynolds stresses at that latitude.

Discrepancies in observation-based conjectures about the mechanism of wave generation did not find an ultimate explanation through the use of numerical models. *Philander* [1976, 1978] used a 1.5-layer model to show that oscillations with characteristics similar to the observed TIWs derive their energy through barotropic in-

[1]Now at Istituto di Scienze dell'Atmosfera e dell'Oceano, CNR, Bologna, Italy.

[2]Now at Department of Earth and Atmospheric Sciences, University of Alberta, Edmonton, Alberta, Canada.

Paper number 1999JC900226.
0148-0227/99/1999JC900226$09.00

stability arising from the latitudinal shear between the SEC and the NECC. An energy analysis of a numerical simulation performed using a multilevel model [*Cox,* 1980] forced with monthly varying winds confirmed that the barotropic instability is the primary source of energy of the TIWs but that the unstable meridional shear is the one between the EUC and the northern branch of the SEC. This energy analysis also indicated that baroclinic instability represents an important energy contribution to the growth of the oscillations. The ratio between the barotropic and the baroclinic production is $\sim 3/2$. The westward propagating eddies produced by *Semtner and Holland's* [1980] multilevel model forced with a constant and steady wind stress derived their energy exclusively through baroclinic instability. This model, as opposed to Cox's model, does not simulate the NECC. Similar to Cox's model, in Semtner and Holland's model, there is evidence of barotropic instability in the equatorial region, but the authors believe that is exclusively associated to low-frequency meanders of the Equatorial Undercurrent (EUC) and not to the westward propagating eddies. The baroclinic nature of TIWs is supported by a midlatitude analysis of the baroclinic instability of a 2.5-layer system on a β plane centered at 5°, which indicates a possibility for baroclinic instability with a maximum growth rate for waves of 780 km [*Schopf,* 1981]. Recently, *McCreary and Yu* [1992] used a 2.5-layer model to show that the equatorial temperature front is important in generating TIWs. In this study the instability, which involves conversion of mean potential energy associated with the variable upper layer temperature front to eddy potential energy, is called frontal instability. *Yu et al.'s* [1995] energy analysis indicates that frontal instability as well as barotropic instability associated with the SEC shear contribute to the growth of TIWs in a linearized version of the 2.5-layer model.

In a recent study, *Proehl* [1996] suggests that the locations of the critical layers within the fluid might be the controlling factors for the dispersion and growth of the TIWs according to the overreflection theory. He proved this hypothesis for temporally and zonally invariant zonal flows in which cases he also showed that the instabilities draw their energy through varying mixes of baroclinic, barotropic, and Kelvin-Helmholtz mechanisms. He concluded that any attempt to classify the instabilities through these energy conversions is misleading. However, in a very recent work, *Qiao and Weisberg* [1998] examined the energetics of the waves detected during the Tropical Instability Wave Experiment (TIWE) through the use of the traditional energy conversions and found that barotropic instability is the main energy source for TIWs. They showed that both the SEC and the EUC are important for the waves to develop and that the baroclinic instability due to the mean meridional temperature gradient is small compared to the barotropic instability. However, they note that their analysis is limited to a latitudinal band between 2°N and 2°S at 140°W and carefully conclude that baroclinic processes might be enhanced farther east, where the waves are more energetic, and away from the equator.

The relative importance of the barotropic versus the baroclinic conversions, the possibility of having two spatially and/or temporally decoupled instabilities versus a single instability arising from two simultaneous (barotropic and baroclinic) instability processes, and the role played by the NECC are three of the important issues that motivate this study. A multilevel general circulation model configured for the equatorial Pacific Ocean and forced with steady summer winds [*Masina and Philander,* this issue] (hereinafter referred to as MP99) is able to reproduce instability waves that are similar to the observed TIWs. We study the generation and propagation mechanisms of TIWs developed in the numerical simulation of the Pacific Ocean through a perturbation (deviation from the time mean) energy analysis. We follow the approach that has been recently used to study the growth and propagation of baroclinic disturbances in the atmosphere, both in actual cases and idealized numerical simulations [e.g., *Orlanski and Katzfey,* 1991; *Chang and Orlanski,* 1993]. The diagnostics of local energetics show that the growth of atmospheric cyclones is a combined product of baroclinic processes and convergence of energy fluxes from upstream decaying energy centers. This process explains the presence of localized waves in the atmosphere observed far downstream from a strong baroclinic source. We apply this local energy analysis for the first time to the ocean in order to explain the growth and propagation of TIWs in the Pacific Ocean.

In section 2 we briefly present the results of a numerical experiment in which TIWs are generated and a discussion about the latitudinal variability of the simulated unstable waves. The eddy kinetic energy equation is derived in section 3. Sources and sinks of eddy kinetic energy and the processes which control its propagation and redistribution in the model domain are investigated in the same section. In section 4 we discuss the energy redistribution inside the domain via the eddy pressure flux divergence. In section 5 we examine the life cycle of the waves through the analysis of the time evolution of the energetics involved during the generation and propagation of the unstable waves. Finally, we conclude with a discussion in section 6.

2. Wind-Forced Numerical Simulations of the Pacific Ocean

Motivated by the data that have been collected in the Atlantic and Pacific Oceans on TIWs [e.g., *Legeckis,* 1977; *Weisberg,* 1979] a few attempts have been made to numerically simulate realistic instability waves [e.g., *Cox,* 1980; *Semtner and Holland,* 1980]. MP99 have been able to simulate TIWs numerically using a primitive equation general circulation model forced with

steady winds. The simulated waves show characteristics very similar to those observed in reality. All the details about the model setup and the intial conditions used are given by MP99.

One of the most interesting features of the TIWs is their latitudinal structure and, in particular, their asymmetry about the equator. The oscillations grow and develop on either side of the equator but not in a symmetric way (MP99, Figure 5). Two different structures are evident: One is localized around 3°N in the region of the SEC, and the second one looks very much like a mixed Rossby-gravity mode symmetric about 1°S. This last structure grows in the boundary region between the EUC and the SEC and is phase locked to the northern one. The energy analysis (section 3) will reveal whether the oscillations are really a superposition of two phase-locked, westward propagating unstable modes grown at two different latitudes or if there is only one unstable mode north of the equator that excites a neutral wave confined to a latitudinal waveguide south of the equator. The last hypothesis is clearly quite unlikely since, in the case of a neutral wave trapped to a waveguide, energy would not be allowed to come in from other regions and therefore it would not be possible to explain the mechanism of phase locking between the two modes.

The numerical simulation of MP99 also shows the presence of unstable oscillations in the central Pacific Ocean south of the equator. These instabilities have a phase speed drastically lower than the phase speed of the oscillations generated in the eastern Pacific north of the equator but have a similar two-peak structure (MP99, Figure 7). The energy analysis described in section 3 will also explain the nature of the low-frequency mode which develops south of the equator.

3. Eddy Kinetic Energy Budget

The traditional interpretation of the energy cycle in terms of conversion terms and flux vectors has been questioned [i.e., *Plumb,* 1983; *Hayashi and Young,* 1987] after more recent reformulations of the eddy mean flow interactions [*McIntyre,* 1980]. In particular, *Plumb* [1983, p.1685] pointed out that "one cannot place any absolute significance on individual conversion or flux terms." For example, the traditional source of energy for baroclinic instability is "via" the conversion between the available potential energy of the mean state and the eddy available potential energy, but this term is identically zero if a new energy cycle using the transformed Eulerian mean equations is considered. Another example is the study of the energetics of barotropic equatorial jets by *Marinone and Ripa* [1984]. They pointed out that any conclusions derived from the spatial structure of the conversion term between the eddy kinetic and the eddy potential energy may be misleading since two different functions can have the same volume integral. The same lack of definiteness applies to the flux terms. A nonzero divergence of the traditional "energy flux" $\overrightarrow{v'p'}$ does not necessarily indicate any increase of wave activity since it can be exactly cancelled by a conversion term. However, *Plumb's* [1983] final remark was that ambiguities appear in all the possible formulations of the energy budget only if one uses only individual terms instead of the total contributions of the fluxes and conversions within the overall context of the particular energy analysis used.

In an effort to understand the energetics of the oscillations generated in the numerical simulation of the Pacific Ocean, we perform an energy analysis of the simulation, and as suggested by *Plumb* [1983], we analyze each flux and conversion term. All the classical energy analyses are based on deviations from zonal or time mean flows and therefore require either a large domain for the zonal mean or a long time series for the time mean. We chose to define the perturbations as deviations from the time mean state because of the difficulties in defining a meaningful zonal mean basic state. The waves develop only in a particular region of the domain, and a zonal mean calculated on the whole length of the domain would not be representative of the basic state seen by any particular wave. An average flow calculated for a period of 1 year can certainly be considered steady in our case since the wind stress that we used to force the model is steady and does not induce any significant variability at frequencies lower than the frequency characteristic of the TIWs (see MP99). In this paper, for brevity and convenience, we refer to the time mean deviation fields as eddies or TIWs.

The eddy kinetic energy equation is derived from the horizontal equations of motion which, in Cartesian coordinates, can be written as follows:

$$\frac{d\vec{v}}{dt} + f\vec{k} \times \vec{v} = -\frac{1}{\rho_0}\vec{\nabla}p + A_{MH}\nabla^2\vec{v} + (A_{MV}\vec{v}_z)_z, \quad (1)$$

where $\vec{v} = (u\vec{i} + v\vec{j})$, $d/dt = (\partial/\partial t) + u(\partial/\partial x) + v(\partial/\partial y) + w(\partial/\partial z)$ and $\vec{\nabla}$ is the horizontal divergence operator $(\partial_x\vec{i} + \partial_y\vec{j})$. We choose to retain the vertical component of the advection because this term can be as large as the horizontal advection for the time mean deviation fields.

The horizontal and vertical viscosity coefficients are A_{MH} and A_{MV}, respectively. Each variable can be decomposed into a time independent (mean) part and the deviation from this time mean:

$$\vec{v}(x,y,z,t) = \vec{V}(x,y,z) + \vec{v'}(x,y,z,t), \quad (2)$$

$$w(x,y,z,t) = W(x,y,z) + w'(x,y,z,t), \quad (3)$$

$$p(x,y,z,t) = P(x,y,z) + p'(x,y,z,t). \quad (4)$$

A further decomposition of perturbation pressure into external (sea surface pressure p_S) and internal (hydro-

static pressure p_h) components is performed according to

$$p'(x,y,z,t) = p_S(x,y,t) + p_h(x,y,z,t). \quad (5)$$

Time-averaged fields have been obtained through averaging the last 360 days of integration of the numerical model.

If we apply the above decomposition to each variable in (1) and then take the time mean, we obtain the time mean momentum equation as follows:

$$\frac{D\vec{V}}{Dt} + f\vec{k}\times\vec{V} = -\frac{1}{\rho_0}\vec{\nabla}P - \overline{\vec{v'}\cdot\vec{\nabla}\vec{v'}} - \overline{w'\vec{v'}_z} + A_{MH}\nabla^2\vec{V} + (A_{MV}\vec{V}_z)_z, \quad (6)$$

where

$$\frac{D}{Dt} = U\frac{\partial}{\partial x} + V\frac{\partial}{\partial y} + W\frac{\partial}{\partial z} \quad (7)$$

and the time mean of the perturbations is zero by construction.

In (6) an overbar is used to indicate the time mean of terms that are a combination of variables. The total momentum equation minus the time mean gives the momentum equation for the time deviation

$$(\frac{\partial}{\partial t} + U\frac{\partial}{\partial x} + V\frac{\partial}{\partial y} + W\frac{\partial}{\partial z})\vec{v'} + \vec{v'}\cdot\vec{\nabla}\vec{V} + w'\vec{V}_z + \vec{v'}\cdot\vec{\nabla}\vec{v'} + w'\vec{v'}_z - \overline{\vec{v'}\cdot\vec{\nabla}\vec{v'}} - \overline{w'\vec{v'}_z} = -f\vec{k}\times\vec{v'} - \frac{1}{\rho_0}\vec{\nabla}p' + A_{MH}\nabla^2\vec{v'} + (A_{MV}\vec{v'}_z)_z \quad (8)$$

The equations for mean kinetic energy $K_M = 1/2\rho_0\vec{V}\cdot\vec{V}$ and eddy kinetic energy $K_e = 1/2\rho_0\vec{v'}\cdot\vec{v'}$ are obtained by multiplying (6) by $\vec{V}$ and (8) by $\vec{v'}$, respectively.

The equation for K_e is thus given by

$$\frac{\partial K_e}{\partial t} + \vec{V}\cdot\vec{\nabla}K_e + WK_{ez} + \vec{v'}\cdot\vec{\nabla}K_e + w'K_{ez} = -\vec{v'}\cdot\vec{\nabla}p' + \rho_0[-\vec{v'}\cdot(\vec{v'}\cdot\vec{\nabla}\vec{V}) - \vec{v'}\cdot(w'\vec{V}_z) + \vec{v'}\cdot\overline{(\vec{v'}\cdot\vec{\nabla}\vec{v'})} + \vec{v'}\cdot\overline{(w'\vec{v'}_z)} + A_{MH}(\vec{v'}\cdot\nabla^2\vec{v'}) + \vec{v'}\cdot(A_{MV}\vec{v'}_z)_z]. \quad (9)$$

The terms on the left-hand side of (9) are the local tendency, the total (horizontal plus vertical) advection by the mean flow, and the total advection by the eddies of K_e, respectively . The first term on the right-hand side of (9) is the pressure work done by the eddies. The second and third terms are the horizontal and vertical deformation work terms, respectively. The fourth and the fifth terms on the right-hand side of (9) are zero in the time mean. Finally, the last two terms represent the horizontal and vertical dissipation by the eddies, respectively.

If we apply the same decomposition described by (2)-(4) to the density $\rho(x,y,z,t)$ and substitute it into the vertical equation of motion under the hydrostatic approximation, the time deviation component becomes

$$p'_z = -\rho' g. \quad (10)$$

Equation (10) and the time deviation of the continuity equation,

$$\vec{\nabla}\cdot\vec{v'} + w'_z = 0, \quad (11)$$

can be used to write the pressure work term as

$$-\vec{v'}\cdot\vec{\nabla}p' = -\vec{\nabla}\cdot(\vec{v'}p') - (w'p')_z - g\rho'w'. \quad (12)$$

The first two terms in (12), whose sum is equal to $-\vec{\nabla}_3\cdot(\vec{v'_3}p')$, where $\vec{v'_3} = u'\vec{i} + v'\vec{j} + w'\vec{k}$, redistribute K_e spatially and are identically equal to zero when averaged over the volume. The last term of (12) represents the rate of work done by the vertical velocity against buoyancy and represents the energy conversion between P_e, where P_e is the eddy available potential energy, and K_e. For a constant value of the term $-\vec{v'}\cdot\vec{\nabla}p'$, the value of the total divergence of the eddy pressure flux, i.e., $-\vec{\nabla}_3\cdot(\vec{v'_3}p')$, determines the value of the term $-g\rho'w'$, i.e., the vertical motion of the mass field. When the term $-g\rho'w'$ is positive, it represents the conversion of eddy available potential energy P_e into eddy kinetic energy K_e

$$P_e \rightarrow K_e. \quad (13)$$

This conversion is commonly known as baroclinic conversion.

When the horizontal deformation work terms in (9) are positive, they represent the conversion of mean kinetic energy K_M into eddy kinetic energy K_e

$$K_M \rightarrow K_e. \quad (14)$$

Such an energy transfer is commonly referred to as barotropic conversion. Also, when the vertical deformation work terms in (9) are positive, the energy conversion is in the same direction, i.e., from mean kinetic energy to eddy kinetic energy, and is referred as Kelvin-Helmholtz conversion. The barotropic, baroclinic, and Kelvin-Helmholtz conversions represent possible sources of eddy kinetic energy. In section 4 we analyze the time mean of these conversion terms to determine the nature of the instabilities observed in the Pacific simulation.

The eddy kinetic energy distribution reflects the region of eddy activity. Therefore, in order to better localize the oscillations and prove some of the hypotheses concerning the energy propagation that we advanced in

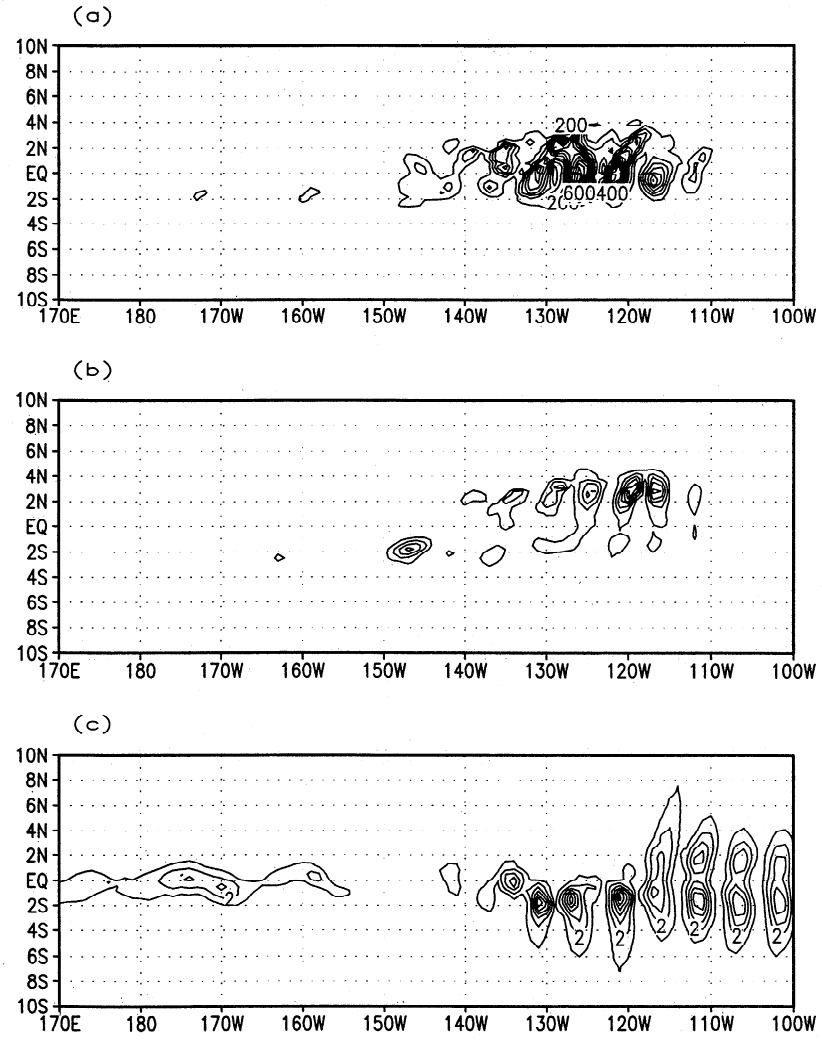

Figure 1. Snapshot at t=20 days of horizontal sections of eddy kinetic energy at (a) 5 m (contour interval (CI) is 100 dyn/cm^3), (b) 95 m (CI is 100 dyn/cm^3), and (c) 1800 m (CI is 1 dyn/cm^3).

the previous section we calculate the eddy kinetic energy and its time mean in the model domain. A snapshot of eddy kinetic energy at three different model levels is shown in Figure 1. At the first model level (5 m) the horizontal distribution of eddy kinetic energy coincides with that of the fluctuations observed in the temperature field (MP99; see their Figure 1b for comparison). The eddy kinetic energy is confined between 2°S and 4°N where the southern and northern temperature fronts, respectively, are located. The eddy kinetic energy centers west of 150°W and and around 2°S (although isolated and relatively weak) indicate that the eddy activity south of the equator has a longer zonal extension than north of the equator. Below the surface (Figure 1b) at 95 m the eddy kinetic energy decreases with respect to the surface and becomes confined mostly north of the equator. South of the equator, the magnitude of the eddy kinetic energy is comparable to the values north of the equator only near 148°W. At z=1800 m (Figure 1c) the eddy kinetic energy magnitude decreases by 2 order of magnitudes with respect to the values found above the thermocline, but its horizontal distribution shows that energetic signals are present in the far eastern and the far western Pacific. This signal suggests that the unstable eddies generated close to the surface excite neutral equatorial waves which propagate downward both to the east and to the west of the instability region [*Cox*, 1980].

The time-averaged eddy kinetic energy provides a statistical representation of the spatial distribution of the eddies. In Figure 2 we show two vertical sections at 130° and 170°W of the eddy (contour) and mean (shaded area) kinetic energy. For clarity, the section is limited to the uppermost 13 model levels (300 m) where most of the eddy kinetic energy is confined. In Figure 2a the mean kinetic energy K_M clearly shows where the mean flow is localized. For example, in this case the K_M maximum coincides with the core of the EUC. The vertical distribution of K_e shows two distinct maxima on either side of the equator indicating that the eddies

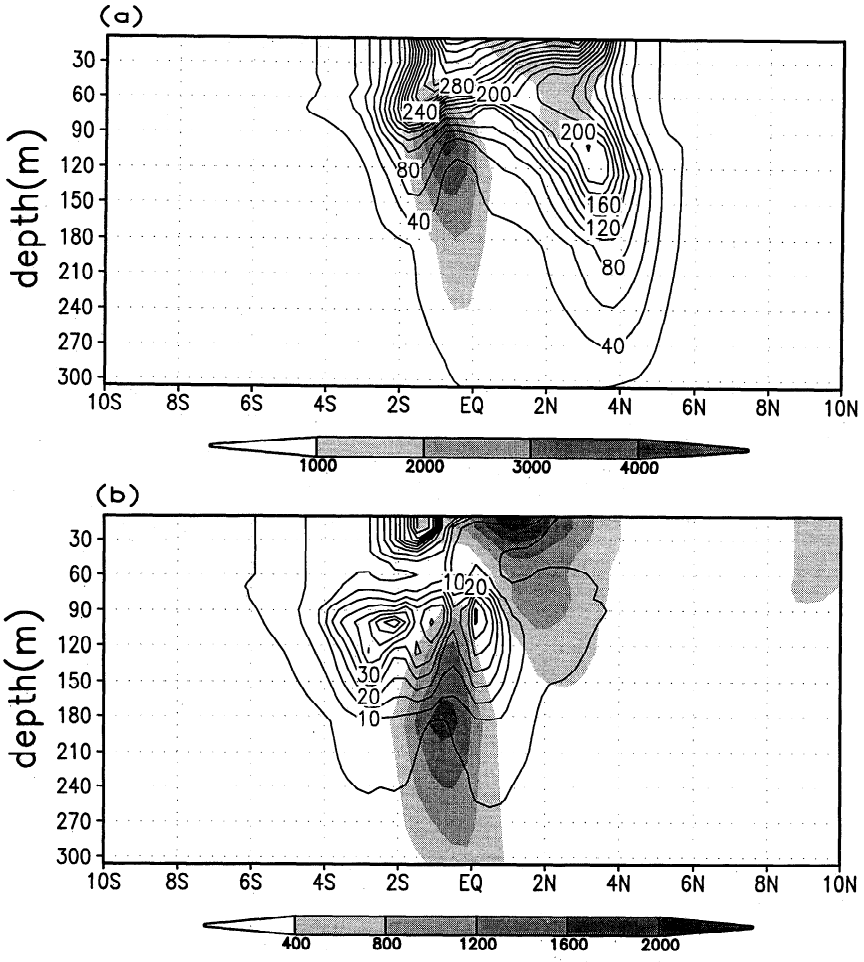

Figure 2. Depth-latitude sections of time mean kinetic energy (shaded) and time mean eddy kinetic energy (contour) at (a) 130° and (b) 170°W. For the mean kinetic energy the CI is 400 dyn/cm^3 in both plots. For the eddy kinetic energy the CI is 20 dyn/cm^3 in Figure 2a and 10 dyn/cm^3 in Figure 2b.

are decoupled below the surface. The same figure shows that the eddies are confined to the upper ocean and, in particular, in the mixed layer. At this longitude the thermocline is asymmetric about the equator, and this asymmetry is reflected in the K_e distribution, which extends deeper in the region of the SEC north of the equator where the thermocline is deeper (180 m).

Figure 2b is identical to Figure 2a, but the cross section is taken at 170°W; that is, the central longitude of the region at which the phase speed of the TIWs decreases drastically. At this longitude, K_e is confined mainly south of the equator. North of the equator, there is only one secondary maximum in K_e localized between the EUC and the SEC. South of the equator the K_e absolute maximum is confined at the surface between 1° and 2°S in the southern branch of the SEC. In the northern branch of the SEC the eddy activity is clearly very weak at this longitude. Below the surface at $\sim$ 100 m, another K_e maximum is localized between the EUC and the southern branch of the SEC.

In Figure 3a, K_M and K_e are shown as a function of longitude and depth at 2°N. The maxima of the two fields coincide and are localized at the surface at 130°W. Below the surface, two secondary K_e maxima are present at a depth of 80 m (one at $\sim$ 120° and the other at $\sim$ 135°W), suggesting that the K_e might propagate downward to the east and to the west of the surface maximum. This downward propagation is more clearly demonstrated by the vertical distribution of K_e at the equator (Figure 3b). At this latitude the K_e maximum is localized at the surface between the northern branch of the SEC and the EUC. Below the surface the K_e pattern shows that part of the energy is distributed downward and westward (remaining above the EUC) and another part extends to deeper levels in the east. Even more clearly, at 2°S (Figure 3c) the K_e distribution in longitude and depth shows a preference for the K_e to be confined above the EUC and to descend with the westward deepening of the EUC.

3.1. Barotropic and Baroclinic Instability

The horizontal and vertical deformation work terms (represented by the second and third terms on the right-hand side of (9), respectively) express the transfer be-

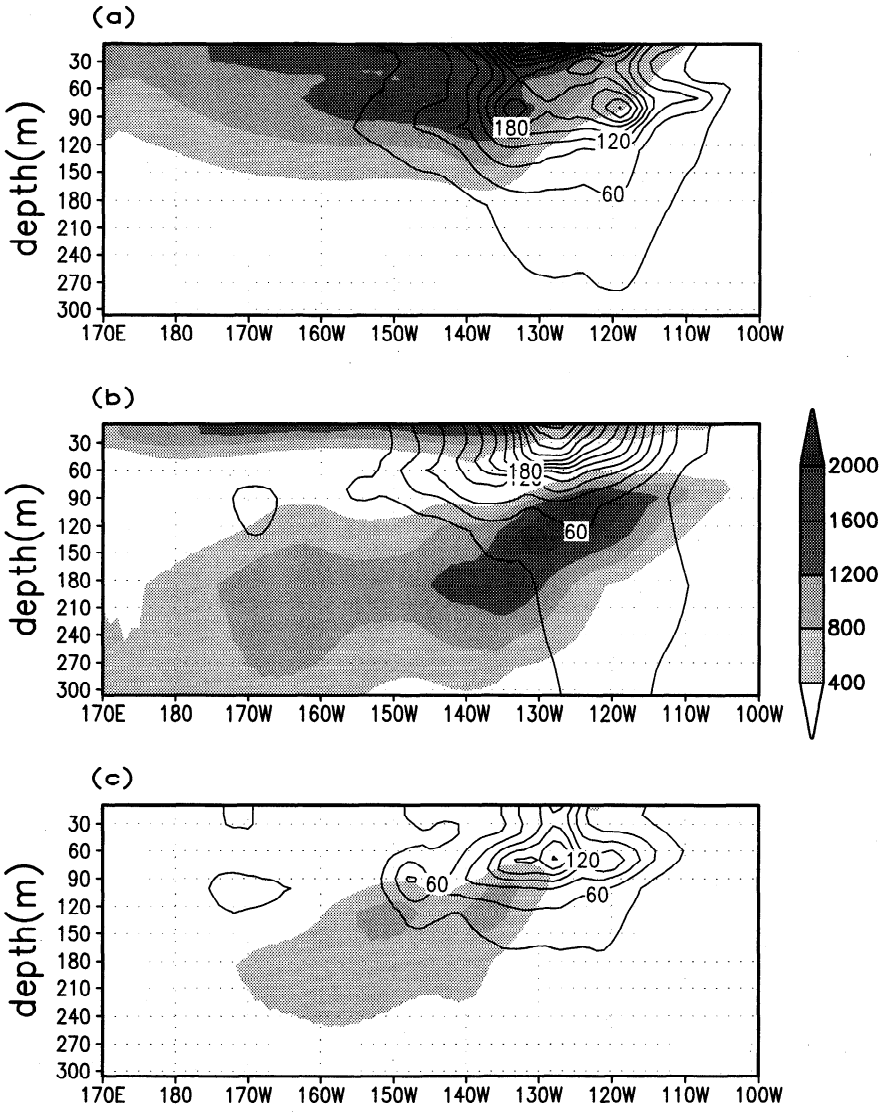

Figure 3. Depth-longitude sections of time mean kinetic energy (shaded) and time mean eddy kinetic energy (contour) at (a) 2°N, (b) the equator, and (c) 2°S. For the mean kinetic energy the CI is 400 dyn/cm^3, and for the eddy kinetic energy the CI is 30 dyn/cm^3 in all plots.

tween the mean kinetic and eddy kinetic energies. In the equatorial region, where the circulation is dominated by zonal flow, the dominant time mean deformation work term is $-\overline{u'v'}(\partial U/\partial y)$. In this region the variations in V mainly arise because of the wave transient and are normally smaller than $\partial U/\partial y$. The term $g\overline{\rho'w'}$ is present, with opposite sign, in the time mean eddy kinetic energy equation (when the decomposition written in (12) is used in (9)) and in the time mean eddy potential energy equation and therefore represents the conversion between the eddy kinetic energy and the eddy potential energy (see *Peixoto and Oort* [1992] for the derivation of the eddy potential energy equation).

Horizontal sections of these two terms are shown, with the same contour interval, at z=5 m (Figures 4a and 4b). At the uppermost level of the model the magnitude of the two terms is comparable (the ratio between the maximum of $\overline{u'v'}(\partial U/\partial y)$ and the maximum of $g\overline{\rho'w'}$ is 3/2), but the horizontal distribution is significantly different. The term $-\overline{u'v'}(\partial U/\partial y)$ (which we will henceforth call the barotropic term for the sake of brevity) is positive mainly in a narrow band straddling the equator between 150° and 115°W. Another positive region but with smaller values is present north of the equator between 2° and 4°N and between 133° and 123°W. Poleward of the positive regions on both sides of the equator the time mean barotropic conversion term is negative. In the central Pacific near 170°W and 2°S, there is another small region characterized by a weak positive barotropic conversion. At the same level (Figure 4b) the time mean baroclinic conversion term is positive everywhere with maximum values attained between the equator and 5°N and between 145° and 105°W. Positive regions of time mean baroclinic conversion are also evident south of the equator. These regions are isolated, and the values of the baroclinic

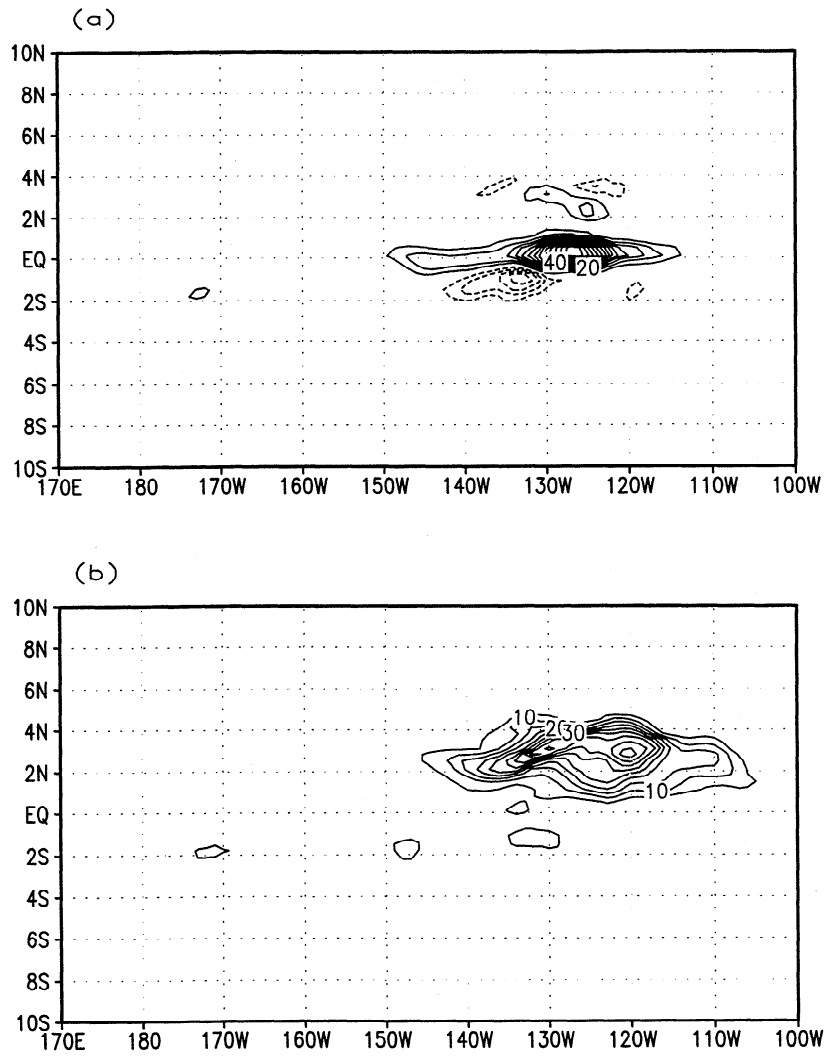

Figure 4. Horizontal sections at 5 m of (a) time mean barotropic conversion and (b) time mean baroclinic conversion. The unit is 10^{-5} cm^2/s^3, and the contour interval is 5 x 10^{-5} cm^2/s^3 in both plots.

conversion are much smaller than those north of the equator. In particular, in the central Pacific Ocean at $\sim$ 170°W and 2°S, there is evidence of barotropic and baroclinic conversion occurring in the same area. In summary, at the surface the main sources of eddy kinetic energy are mean kinetic energy at and very close to the equator and eddy potential energy north of 1°N.

The time mean barotropic and baroclinic terms below the surface at z=95 m (Figures 5a and 5b) have both a magnitude and a horizontal distribution very similar to those near the surface. The magnitude of the barotropic term is $\sim 1/3$ of the surface amplitude, and its maximum is shifted 10° to the west. Another noticeable difference in the eastern Pacific is a shift of the baroclinic conversion term to slightly higher latitudes north of the equator. The isolated eddy region in the central Pacific south of the equator, which at the surface, was characterized by an equal amount of barotropic and baroclinic conversion, at this depth shows only barotropic conversion.

A more complete picture of the vertical distribution of the time mean barotropic and baroclinic conversion terms as a function of latitude in the eastern Pacific (130°W) is given in Figure 6. The maximum barotropic conversion (Figure 6a) is clearly taking place in the upper 150 m in the region characterized by the strong meridional shear between the core of the EUC and the northern branch of the SEC. The meridional shear of the EUC south of the equator has a magnitude comparable to the shear north of the equator but is, nevertheless, not barotropically unstable even if the potential vorticity meridional gradient $\beta - U_{yy}$ changes sign in the vertical in both regions around 1°N and 2°S [*Masina,* 1996]. However, this criterion is a necessary condition for barotropic instability only at middle latitudes under the quasi-geostrophic approximation and in nondivergent conditions [*Kuo,* 1949]. The strong divergent and ageostrophic effects that characterize the equatorial region preclude us from using Kuo's criterion as a strict proof of barotropic instability in the region

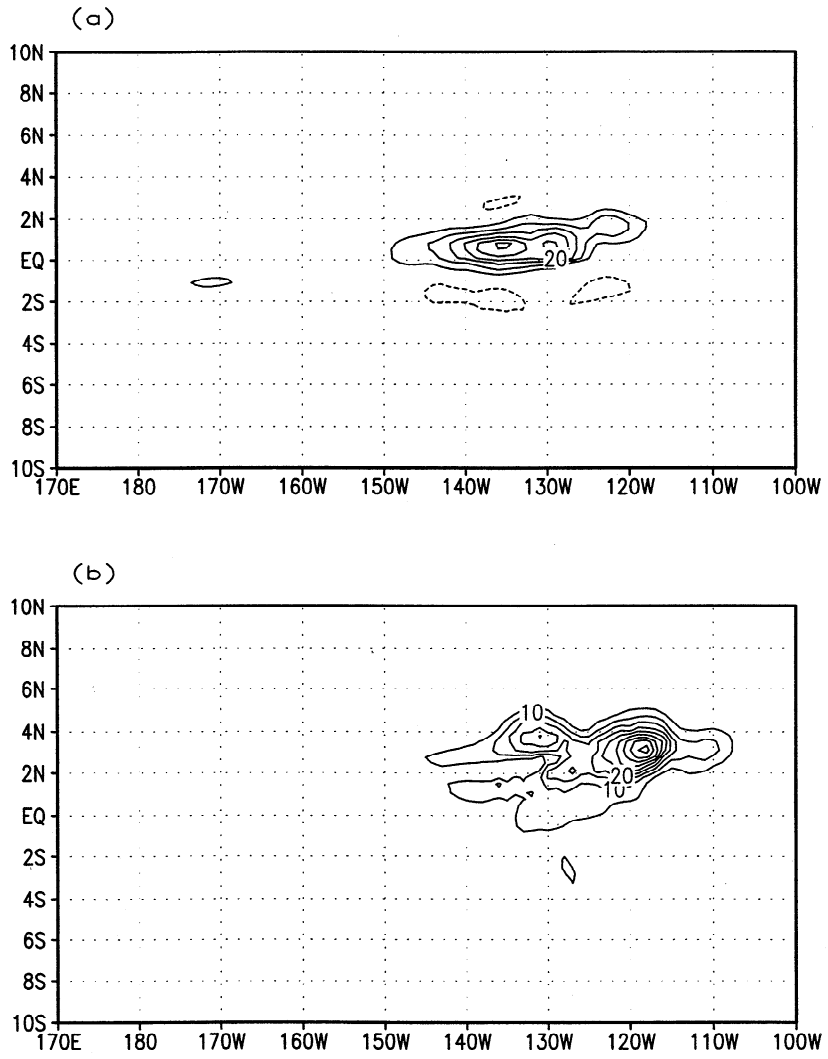

Figure 5. Horizontal sections at 95 m of (a) time mean barotropic conversion and (b) time mean baroclinic conversion in (b). The unit is 10^{-5} cm^2/s^3, and the contour interval is 5 x 10^{-5} cm^2/s^3 in both plots.

close to the equator. Furthermore, this result suggests that the presence of additional horizontal shear associated with the SEC is crucial for the eddies to grow by barotropic processes. The meridional shear between the SEC and the NECC at this longitude is not strong enough to trigger barotropic instability. However, it is necessary to point out that the maximum speed of the simulated NECC is 30 cm/s, a speed which is near the lower limit of actual speeds characteristic of the NECC (during some periods of the year this current can be almost as fast as the EUC and reach a velocity of $\sim$ 100 cm/s; see *McPhaden,* [1996] and *Flament et al.* [1996]. On the basis of the present results we would expect that during periods of intense NECC flow, barotropic instability could arise at latitudes poleward of the region where TIWs grow in our numerical simulations. The time mean baroclinic conversion at 130°W (Figure 6b) shows that the maximum conversion of eddy potential energy to eddy kinetic energy occurs between 1° and 5°N in the uppermost 300 m. This is the latitudinal band in which the northern temperature front is focused as a consequence of the wind-driven upwelling and surface divergence. At this longitude the ratio between the maxima of the barotropic and baroclinic conversion terms is 5/4. The development of a weakly stratified mixed layer at the surface of the ocean is another consequence of wind forcing, and in the equatorial region the combination of strong meridional temperature gradient and weak stratification creates a reservoir of eddy potential energy. In fact, the maximum baroclinic conversion at 130°W occurs in the mixed layer (upper 90 m) where the stratification of the fluid is very small. Another region of weak baroclinic conversion is evident between 1° and 2°S in the first 60 m. This region coincides with the location of the southern temperature front. The weaker and shallower nature of the baroclinic conversion south of the equator is consistent with the smaller meridional temperature gradient associated with the southern front and with the shallower mixed layer south of the equator, respectively [*Masina,* 1996].

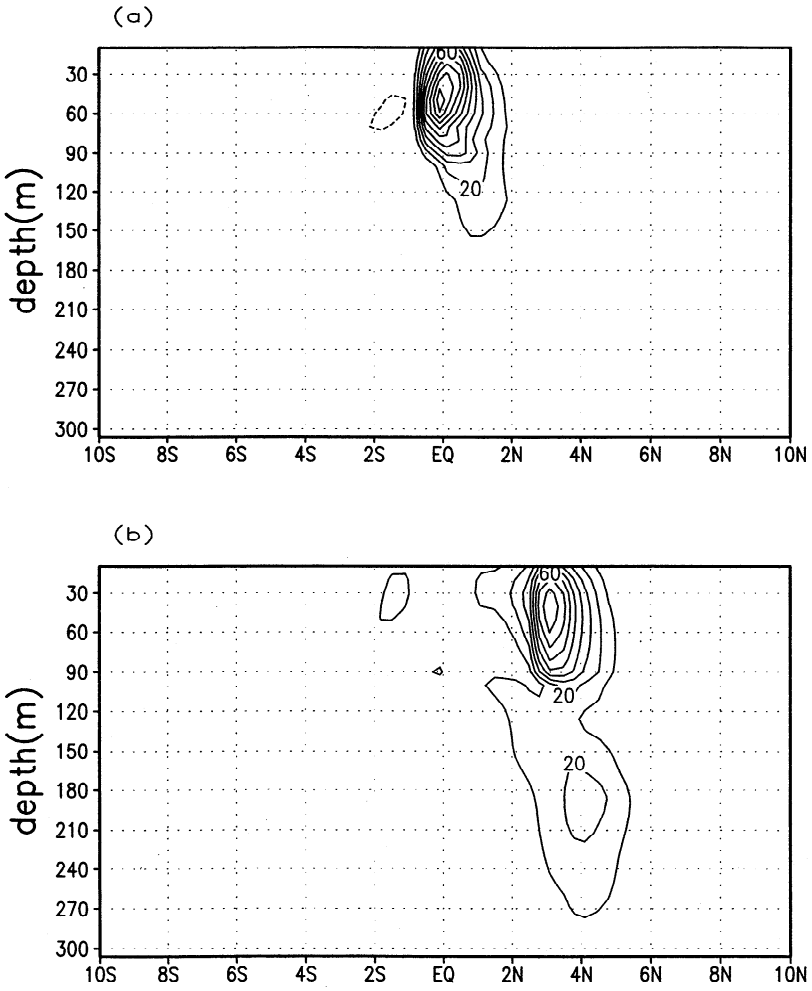

Figure 6. Depth-latitude sections at 130°W of (a) time mean barotropic conversion and (b) time mean baroclinic conversion. The unit is 10^{-5} cm^2/s^3, and the contour interval is 10 x 10^{-5} cm^2/s^3 in both plots.

At 170°W (Figure 7) the vertical distribution of the time mean energy conversion terms is more complex and reflects the differences in the mean flow circulation and the associated thermal field between the eastern and the central Pacific. First of all, we notice that the amplitudes of both the conversion terms is much smaller than those in the eastern Pacific (the contour interval is 10 and 4 times smaller for the barotropic and baroclinic conversion, respectively), indicating that the dynamical and thermodynamical conditions in the eastern Pacific are more likely to be unstable than in the central and western Pacific. The barotropic conversion (Figure 7a) attains two maxima below the surface (which is consistent with the deepening of the EUC toward the west) in two distinct regions. The barotropically unstable region at the equator coincides with the location of the maximum meridional mean flow shear between the EUC and the northern branch of the SEC as in the eastern Pacific, but in the central Pacific this shear occurs at a deeper level because the EUC is deeper. The other barotropic conversion maximum occurs at the southern border of the EUC just below the southern branch of the SEC. The time mean baroclinic conversion at 170°W (Figure 7b) is confined to the upper 100 m between 3° and 1°S, and its magnitude is twice the barotropic conversion magnitude. The asymmetric behavior of the baroclinic conversion about the equator at both 130° and 170°W is consistent with the asymmetric nature of the temperature front in the equatorial region. In fact, in the central and western Pacific the southern temperature front is clearly stronger than the northern front and vice versa in the eastern Pacific (MP99).

The depth-longitude sections (not shown) of the time mean barotropic and baroclinic conversion terms at 2°N and 2°S confirm that the baroclinic conversion strongly dominates over the barotropic conversion at these latitudes. In particular, it is very intense in the upper 120 m in the eastern Pacific north of the equator where it dominates the barotropic signal by 4 times. South of the equator the barotropic conversion is negative in the eastern Pacific and positive in the central Pacific. The baroclinic conversion is positive with two maxima

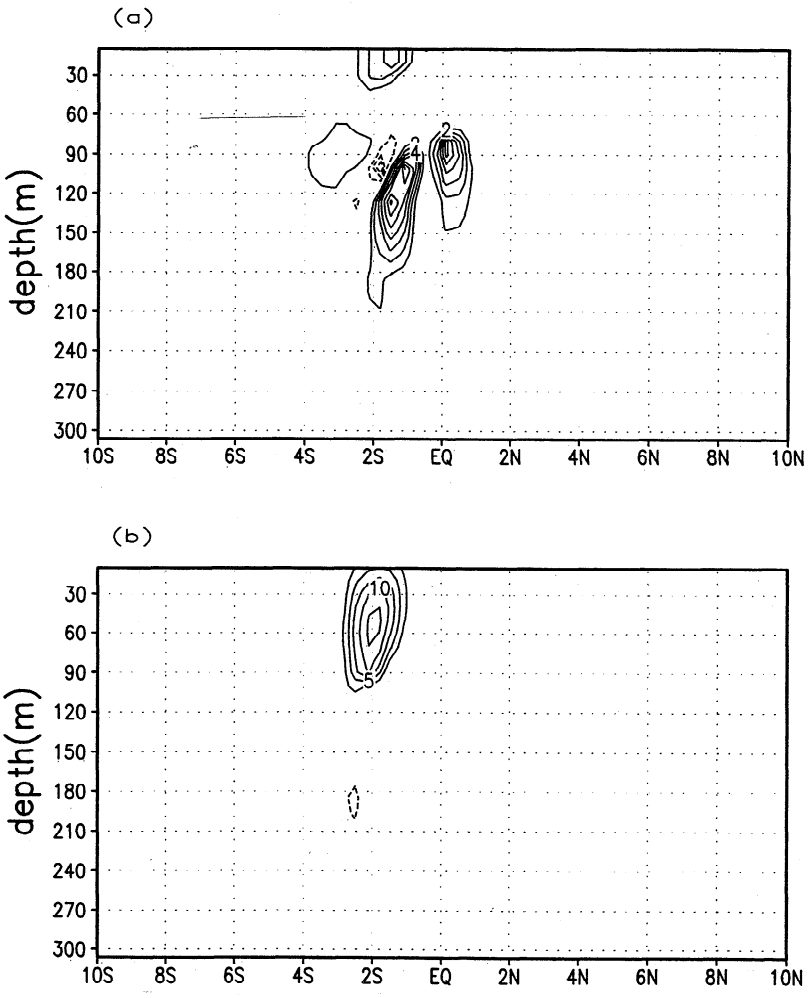

Figure 7. Depth-latitude sections at 170°W of (a) time mean barotropic conversion and (b) time mean baroclinic conversion. The unit is 10^{-5}. Contour interval is 1 x 10^{-5} cm^2/s^3 in Figure 7a and 2.5 x 10^{-5} cm^2/s^3 in Figure 7b.

at 148° and 170°W at 60 m below the surface. At the equator the barotropic conversion term is > 1 order of magnitude larger than the baroclinic conversion term (which, nevertheless, is not zero) along the whole Pacific Ocean.

In conclusion, through a local energy analysis we have demonstrated that in the time mean sense both barotropic and baroclinic conversions are important for the development of TIWs in the Pacific Ocean. In fact, the two phase-locked structures previously identified in the eastern Pacific that determine the structure of TIWs (section 2) have a different nature. The equatorial mode grows through a barotropic instability process that draws on the kinetic energy of the mean flow in the region of strong meridional shear between the EUC and the northern branch of the SEC. On the contrary, the northern mode grows through a baroclinic instability process occurring in a region confined a few degrees north of the equator where the strong temperature front builds up available potential energy that can be used to grow the eddies [*Masina,* 1996]. In our simulated TIWs these two modes occur simultaneously, as opposed to some observations which identify two instabilities at different times [*Luther and Johnson,* 1990]. The oscillations grown in the central Pacific south of the equator have a nature similar to the waves in the eastern Pacific with both barotropic and baroclinic conversions playing an important role but in different regions. In the central Pacific the southern temperature front is baroclinically unstable in the mixed layer, while the mean flow is barotropically unstable below the mixed layer in two regions which coincide with the maximum latitudinal shear between the EUC and the two branches of the SEC.

The results of the local energy analysis are consistent with the results obtained from idealized experiments performed in a channel model [*Masina,* 1996]. When a westward surface parabolic jet with maximum velocity of 100 cm/s is made asymmetric about the equator in order to simulate more realistically the structure of

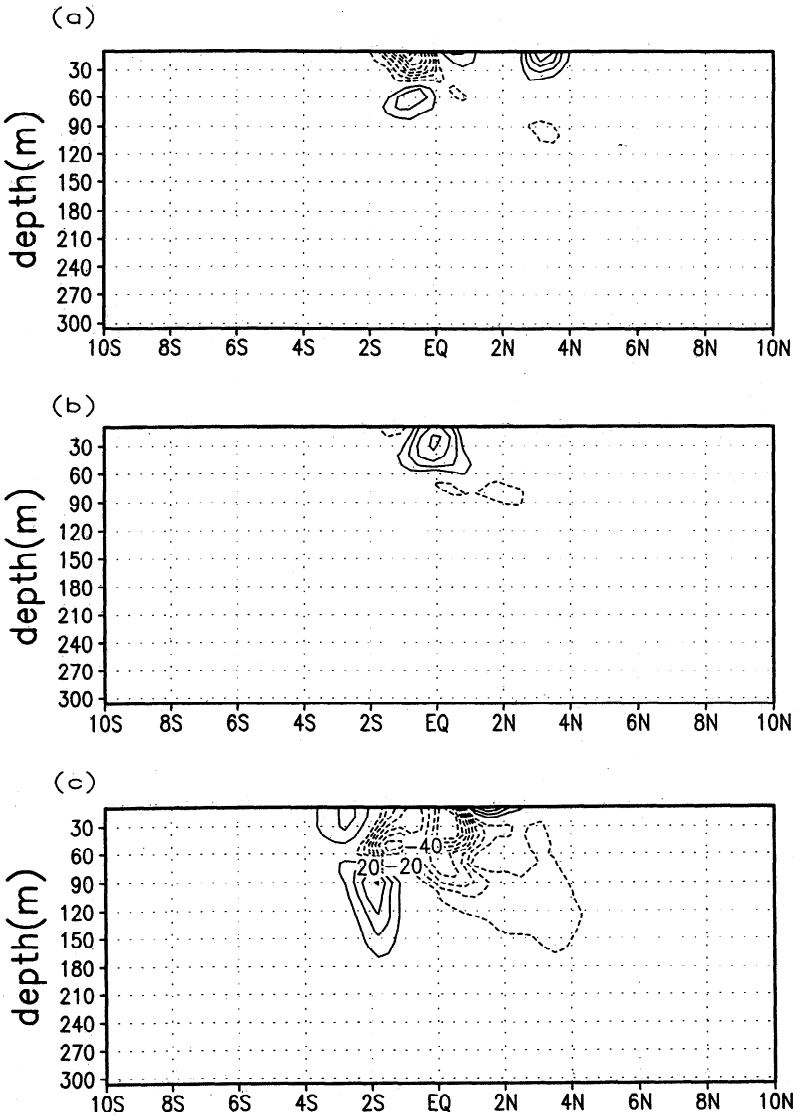

Figure 8. Depth-latitude sections at 130°W of (a) time mean $-vv\partial V/\partial y$, (b) time mean $-uv\partial V/\partial x$, and (c) time mean $-uu\partial U/\partial x$. The unit is 10^{-5} in Figure 8a and 10^{-6} in Figure 8b and 8c. Contour interval is 10 x 10^{-5} cm^2/s^3 in Figure 8a and 10 x 10^{-6} cm^2/s^3 in Figures 8b and 8c.

the SEC in the eastern Pacific, two kinds of instability are generated in a channel model. The oscillations that grow north of the equator have a baroclinic nature, while those generated on and very close to the equator have a barotropic nature. The channel experiments suggest that this two-peak structure can be sustained by an asymmetric SEC alone without the presence of the EUC. The results from the channel experiments [*Masina,* 1996] also proved that for unstable westward jets centered on the equator with the same meridional temperature gradient the available potential energy and the magnitude of baroclinic conversion increase with an increase in depth of the mixed layer. On the contrary, when the mixed layer depth is the same, the system with the largest meridional temperature gradient has the largest available potential energy. These conclusions reveal why, in the eastern Pacific, the waves grow north of the equator while they grow south of the equator in the central Pacific. The mixed layer in the eastern Pacific is twice as deep ($\simeq$ 100 m) north of the equator than south of the equator, and this explains why the southern temperature front, despite having a meridional gradient as large as that north of the equator, is not baroclinically unstable. In the central Pacific the mixed layer is equally deep on either side of the equator, but the meridional temperature gradient along the southern front is larger than along the northern front, allowing the mean flow to become baroclinically unstable only south of the equator.

Finally, the barotropic and baroclinic sources of energy are spatially consistent with the horizontal and vertical distribution of eddy kinetic energy everywhere in the model domain except in one particular region: South of the equator in the eastern Pacific, the time

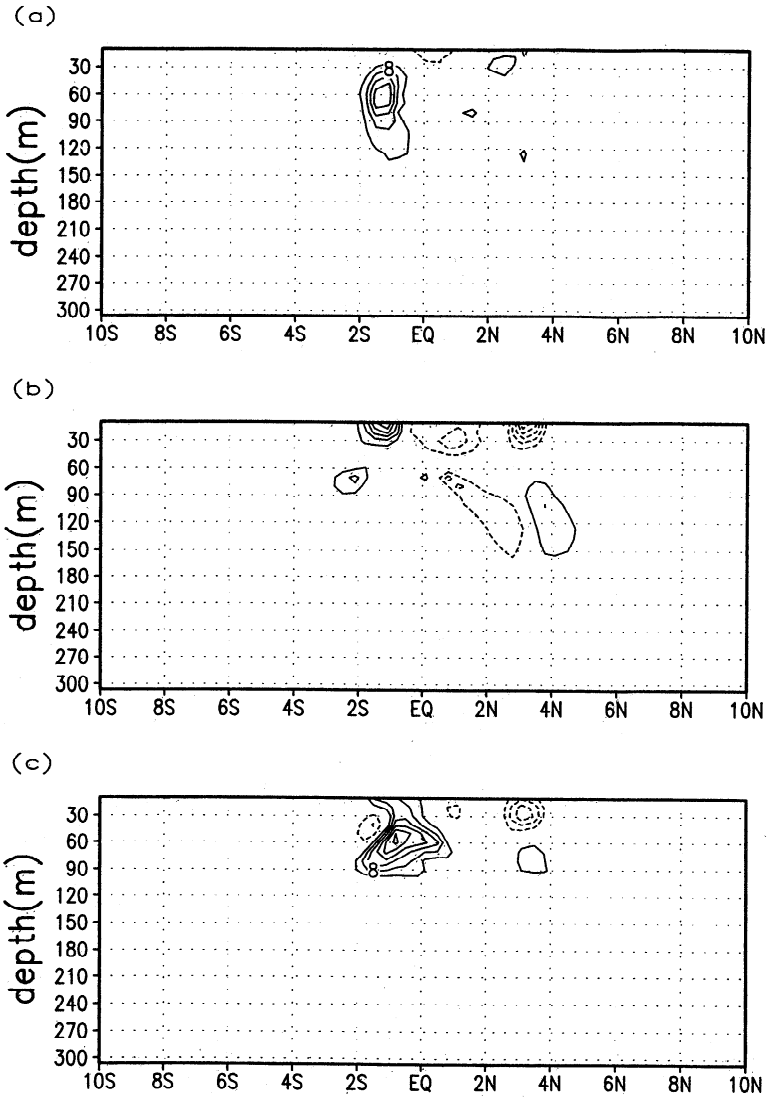

Figure 9. Depth-latitude sections at 130°W of the time mean advection of eddy kinetic energy by (a) the zonal flow, (b) the meridional flow, and (c) the vertical flow. The unit is 10^{-5}, and the contour interval is 4 x 10^{-5} cm^2/s^3.

mean K_e maximum (see Figure 2a) is not explained by either barotropic or baroclinic conversion, and therefore an analysis of the other terms in (9) is required.

3.2. Deformation Work Terms and Advection

Apart from the barotropic conversion term $(-\overline{u'v'}(\partial U/\partial y))$ and the baroclinic conversion term $(-g\overline{\rho'w'})$ that we have analyzed in section 3.1, other possible sources or sinks of eddy kinetic energy are the other horizontal deformation work terms and the vertical deformation work term (second and third terms on the right-hand side of (9)). The time means of these three terms at 130°W are shown in Figure 8. Only the term $-\overline{v'v'}(\partial V/\partial y)$ has a magnitude comparable with the barotropic conversion term (note that the contour interval in Figure 8a is the same as in Figure 6 but is 1 order of magnitude larger than in Figures 8b and 8c). This term is positive, representing a source of eddy kinetic energy, between the equator and 4°N in the upper 50 m. However, this term is smaller than the barotropic term everywhere in the horizontal domain and mainly confined to the uppermost 30 m. Between the equator and 2°S this term is confined to the upper 90 m and switches sign from negative to positive below 50 m. The negative values close to the surface indicate that this term is a sink of K_e, and therefore it is not a candidate able to explain the presence of a time mean K_e signal south of the equator. The other two horizontal deformation work terms, $-\overline{u'v'}(\partial V/\partial x)$ and $-\overline{u'u'}(\partial U/\partial x)$, are negligible. The vertical deformation work term (not shown) is usually negligible in the ocean because of the small eddy vertical velocity, and this has been confirmed in our simulation.

The analysis of all deformation work terms and the

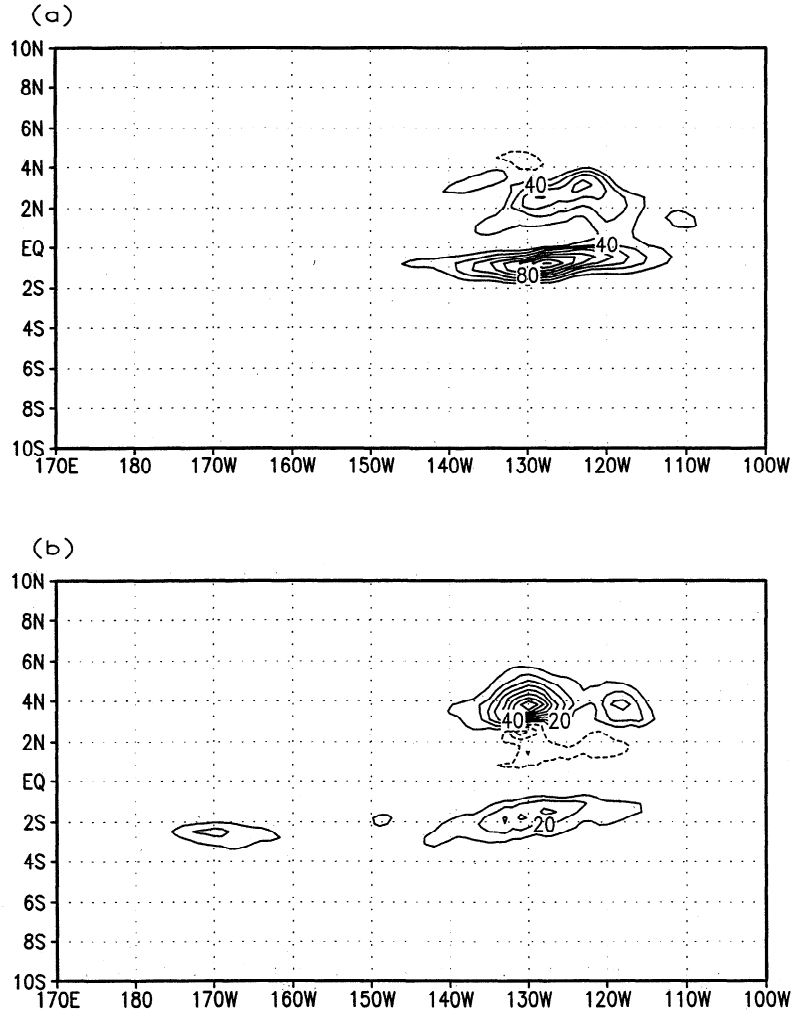

Figure 10. Horizontal sections of the time mean divergence of eddy pressure flux at (a) 5 m and (b) 95 m. The unit is 10^{-5}. Contour intervals are 20 x 10^{-5} cm^2/s^3 in Figure 10a and 10 x 10^{-5} cm^2/s^3 in Figure 10b.

baroclinic conversion term has failed to explain the eddy kinetic energy located in the eastern Pacific south of the equator. Therefore the presence of eddy kinetic energy in that region must be explained through energy propagation or energy redistribution represented by the K_e advection terms (the four last terms on the left-hand side of (9)) and by the divergence of eddy pressure fluxes (first two terms on the right-hand side of (12)), respectively. In Figure 9 we show the total horizontal and vertical advection of K_e (i.e., the sum of advection by the mean flow and by the eddies) at 130°W. The values of the three terms are similar to each other but are much smaller than those of the barotropic conversion term (the contour interval is 4 as opposed to 10 in Figure 6). Both the horizontal and vertical K_e advections are positive between 2°S and the equator, indicating that in the eastern Pacific south of the equator the presence of K_e is partially explained by advection into the region of K_e that has been generated at other latitudes, longitudes, and depths. The vertical advection is the dominant term below the surface between 30 and 90 m, suggesting that K_e is advected from the bottom of the mixed layer to the surface. In the central Pacific at 170°W (not shown), only the vertical advection represents a significant positive term for the K_e redistribution. Nevertheless, advection of K_e by the mean flow and by the eddies cannot explain the K_e maxima south of the equator completely. Another important term for the redistribution and dispersion of K_e is the divergence of the eddy pressure fluxes.

4. Eddy Pressure Flux Divergence

In the atmosphere the eddy geopotential flux has been shown to be very important for the development and decay of cyclone waves. *Orlanski and Katzfey* [1991] showed a clear connection between the ageostrophic pressure flux vector $\vec{v}_a' p'$ and the kinetic energy centers in the energy analysis of the downstream development of an atmospheric cyclon at midlatitudes. Unfor-

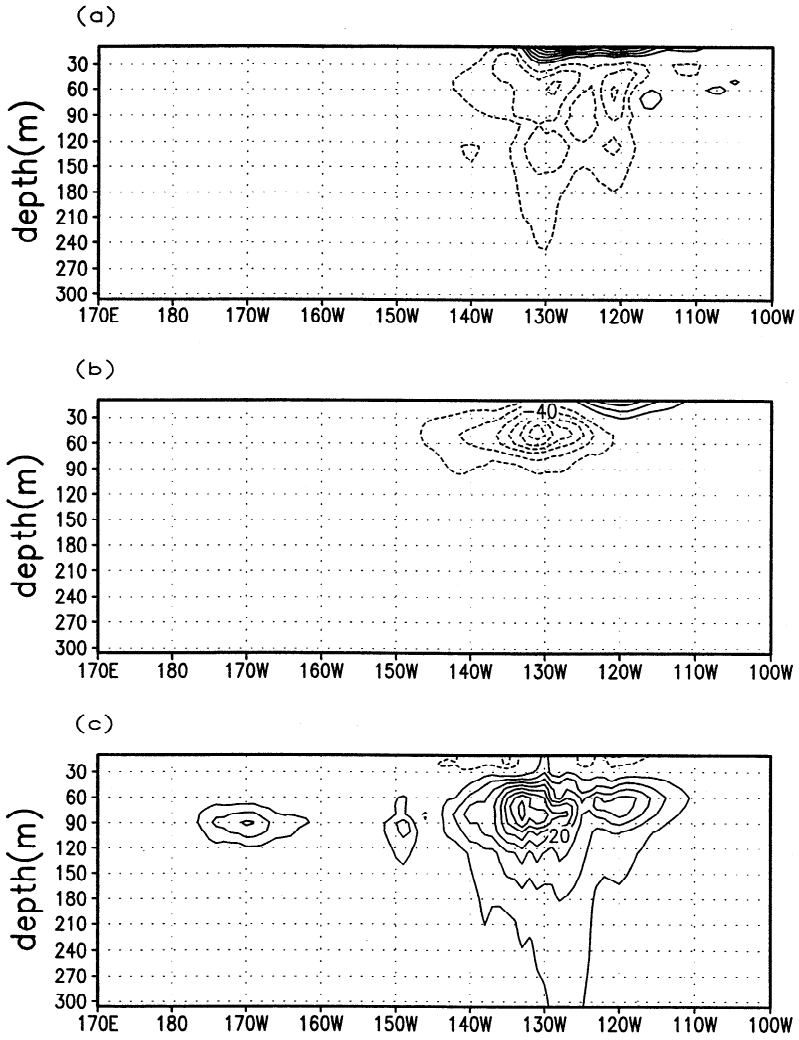

Figure 11. Depth-longitude sections of the time mean divergence of eddy pressure flux at (a) 2°N, (b) the equator, and (c) 2°S. The unit is 10^{-5}. Contour intervals are 10 x 10^{-5} cm^2/s^3 in Figures 11a and 11b and 5 x 10^{-5} cm^2/s^3 in Figure 11c.

tunately, in the equatorial band we cannot define a nondivergent geostrophic velocity, and therefore we cannot try to repeat the analysis of *Orlanski and Katzfey* [1991] in terms of ageostrophic pressure fluxes. However, we can still examine the divergence of the total eddy pressure fluxes. The first term on the right-hand side of (12) is the horizontal divergence of the eddy pressure flux and represents the dispersion of energy. The second term is the vertical eddy pressure flux divergence that redistributes energy vertically and is zero if averaged vertically over the entire domain depth (because the vertical velocity is zero at the surface and at the bottom). The third term is the baroclinic conversion term.

In Figure 10 we show the time mean of the three-dimensional (3-D) divergence of the eddy pressure flux $-\vec{\nabla}_3 \cdot (\vec{v_3'}p')$ (sum of the first two terms on the right-hand side of (12)) at two different depths. At the first model level (z=5 m; Figure 10a) the term $-\vec{\nabla}_3 \cdot (\vec{v_3'}p')$ is strongest between the equator and 2°S and between 145° and 115°W. This term is positive also north of the equator between 135° and 115°W, but its magnitude is much smaller than south of the equator. At 95 m (Figure 10b) the same term reaches its maximum at 4°N and 130°W. It is positive also south of the equator and negative between the equator and 3°N. Another positive region is visible around 170°W between 4° and 2°S. When $-\vec{\nabla}_3 \cdot (\vec{v_3'}p')$ is positive, it means that this quantity represents a source of eddy kinetic energy according to (9) and (12). Three vertical sections of the time mean $-\vec{\nabla}_3 \cdot (\vec{v_3'}p')$ at 2°N, the equator, and 2°S are shown respectively in Figures 11a-c, respectively. From Figure 11 it becomes clear that the role of the divergence of the eddy pressure flux, in the time mean sense, is to "radiate" energy from the regions where K_e is generated through barotropic and baroclinic instabilities

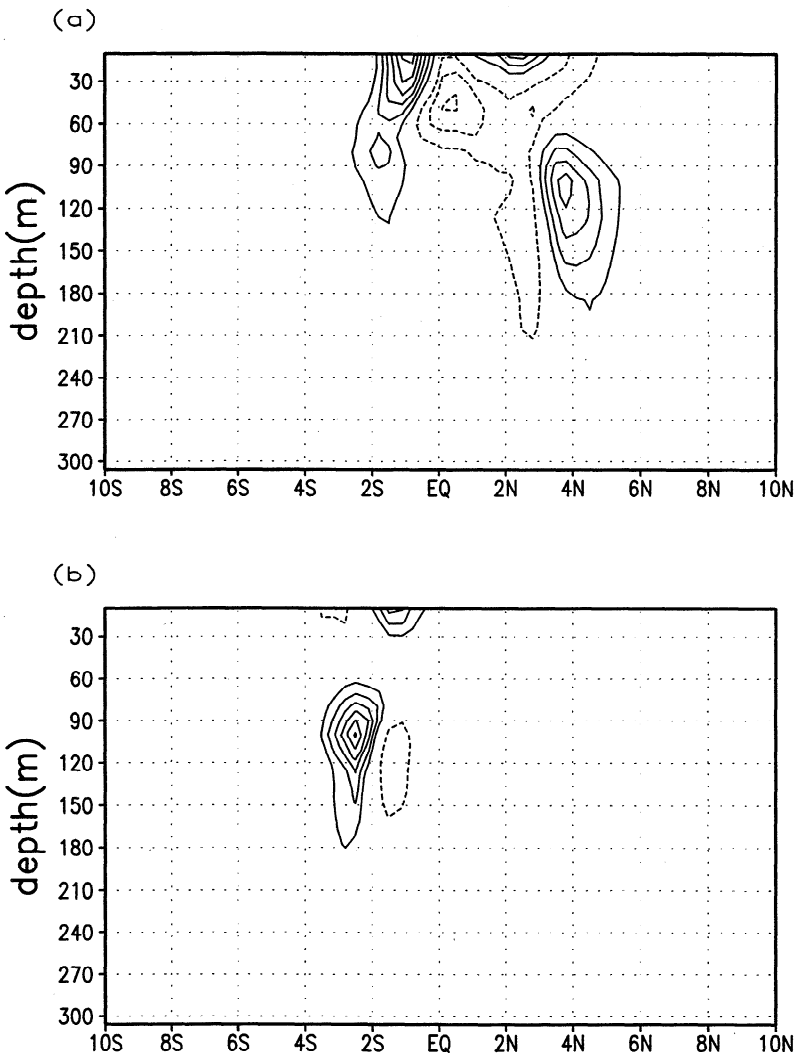

Figure 12. Depth-latitude sections of the time mean divergence of eddy pressure flux at (a) 130° and (b) 170°W. The unit is 10^{-5}. Contour intervals are 20 x 10^{-5} cm^2/s^3 in Figure 12a and 4 x 10^{-5} cm^2/s^3 in Figure 12b.

into other regions. In particular, the eddy pressure flux tends to transport part of the K_e generated between the equator and 4°N (where the quantity $-\vec{\nabla}_3 \cdot (\vec{v_3'} p')$ is negative) southward (south of the equator the quantity $-\vec{\nabla}_3 \cdot (\vec{v_3'} p')$ is positive). This tendency is confirmed by the distribution in depth of $-\vec{\nabla}_3 \cdot (\vec{v_3'} p')$ at two different longitudes in the eastern (130°W: Figure 12a) and central Pacific (170°W: Figure 12b). In the eastern Pacific the eddy pressure flux tends to radiate energy south of the equator in a vertical layer confined between the surface and the thermocline (at $\sim$ 1°S) and poleward of 3°N between 60 and 180 m. In the central Pacific the time mean eddy pressure flux radiates K_e to the surface between the equator and 2°S and below 60 m poleward of 2°S.

In summary, if Figures 6 and 12a are summed, they explain well the time mean K_e distribution at 130°W as a function of latitude and depth (see Figure 2a). K_e that is produced above the thermocline close to the equator through barotropic instability and a few degrees north of the equator through baroclinic instability is partly radiated poleward and downward on both sides of the unstable region. A similar process is seen in the central Pacific. The time mean K_e distribution at 170°W (Figure 2b) arises from a sum of K_e production from barotropic and baroclinic conversions (Figure 7) and from the radiative process determined from the divergence of the total eddy pressure flux.

So far, we have analyzed the time average of some of the terms of (9). The local eddy kinetic tendency $\partial K_e/\partial t$ averaged over 1 year is negligible, and we have shown that the main balance is between the first two terms on the right-hand side of equation (9), i.e., between the deformation work terms, in particular $-\overline{u'v'}(\partial U/\partial y)$, and the pressure work term. However, if we do not perform time average, we can also examine

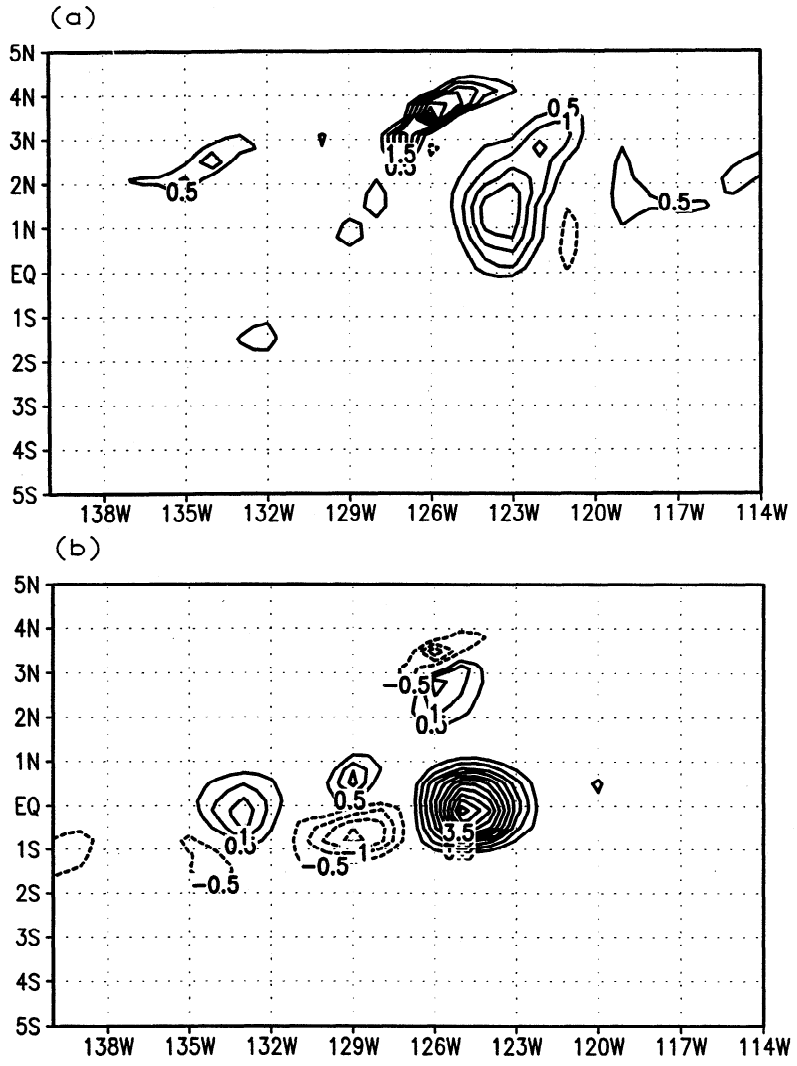

Figure 13. Latitude-longitude snapshot at t=9 days at a depth of 5 m of (a) baroclinic conversion and (b) barotropic conversion. The unit is 10^{-3}. CI is 0.5 x 10^{-3} cm^2/s^3 in both plots.

how the evolution in time of the K_e is determined by the different processes expressed by each term in (9).

5. Life Cycle of TIWs

Chang and Orlanski [1993] showed that convergence and divergence of geopotential fluxes can sometimes dominate the baroclinic and barotropic conversions in the downstream development of atmospheric baroclinic waves. Initially, a wave amplifies through baroclinic conversion, but then it decays through downstream radiation of energy via geopotential flux with barotropic conversion (inverse barotropic cascade) playing only a minor role. This geopotential flux becomes the main source of energy for the development of a downstream wave for which the baroclinic conversion term becomes important only in a subsequent phase. We are now in a position to determine whether the westward propagation of TIWs in the Pacific Ocean is locally dominated by unstable processes or if, as in the atmospheric case, the radiation of energy through the pressure fluxes plays a dominant role.

In Figures 13 and 14 we show snapshots of different quantities at the first model level (z=5 m) in the eastern Pacific at t=9 days. The baroclinic conversion term is shown in Figure 13a, and the barotropic conversion term is shown in Figure 13b. Figure 14 shows the eddy kinetic energy K_e (Figure 14a) and the 3-D divergence of the total eddy pressure fluxes, $-\vec{\nabla}_3 \cdot (\vec{v_3'} p')$ (Figure 14b). Because of the complex vertical structure of the perturbation fields it was preferable not to perform a vertical average in order to retain all possible information about the generation and redistribution of K_e.

The K_e maximum that straddles the equator (Figure 14a) is explained by a combination of an instability process that is mainly barotropic at this latitude (Figure 13b) and divergence of the eddy pressure fluxes (Figure 14b). The K_e maximum north of the equator has the same mixed nature and arises from a combination of K_e production through baroclinic instability

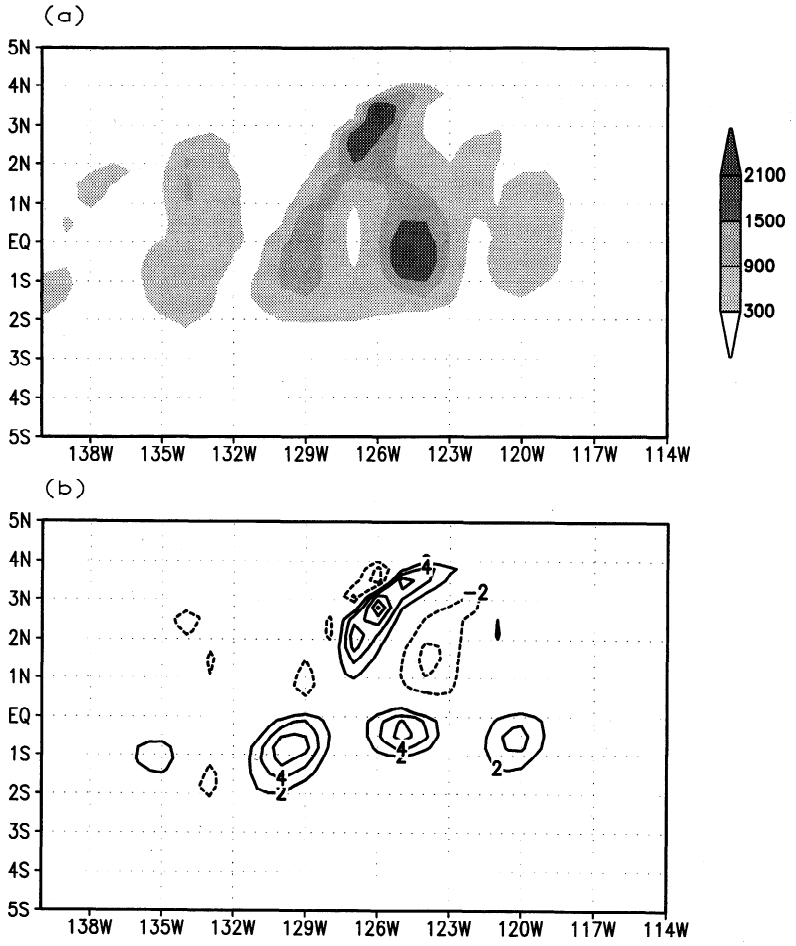

Figure 14. Latitude-longitude snapshot at t=9 days at a depth of 5 m of (a) eddy kinetic energy (shaded) and (b) the divergence of eddy pressure flux. The unit is 10^{-3}. Contour intervals are 600 x 10^{-3} cm^2/s^2 in Figure 14a and 2 x 10^{-3} cm^2/s^3 in Figure 14b.

(Figure 13a) and divergence of the eddy pressure fluxes (Figure 14b). An analysis of the horizontal and vertical divergence of the eddy pressure fluxes separately (the first and second terms on the right-hand side of (12), respectively) shows that the two positive maxima in the convergence field of eddy pressure fluxes (one north of the equator and one south of the equator between 123° and 126°W, where the barotropic conversion is maximum) are explained by the horizontal convergence.

To demonstrate the vertical structure of the energetics of the waves, we show in Figures 15 and 16 the same quantities as in Figures 13 and 14 but at z=95 m. At this depth the baroclinic instability processes play a more important role with respect to the barotropic instabilities almost everywhere inside the domain (see Figures 15a and 15b).

The horizontal distribution of K_e at z=95 m is out of phase with respect to the surface (compare Figure 14a with Figure 16a). All the K_e maxima at 95 m are to the east of the corresponding maxima at the surface. For waves that have a westward phase speed, as is the case for TIWs, this means that the deeper signal leads the surface signal or, in other words, that the deeper signal grows before the surface signal. Moreover, the K_e maxima below the surface are confined near 3°N, and as we demonstrated in section 3.1, the dominant instability process at work north of 1°N has a baroclinic nature. If we combine this result with the evidence that the K_e maxima below the surface north of the equator lead the K_e maxima at the surface, we can finally conclude that the mechanism that triggers the development of TIWs in the eastern Pacific is dominantly baroclinic instability that starts below the surface. The K_e maximum at 123°W below the surface is explained through the convergence of eddy pressure fluxes, probably from the upstream K_e center, and not through baroclinic conversion. The same results have been found at different snapshosts during the time history of the waves.

The energy analysis in the vertical direction helped us to explain the triggering mechanism which determines the wave growth. Now we follow the time evolution of the different energy terms during the westward propagation of the waves in order to understand their life cycle. Figure 17 shows two snapshots in the eastern Pa-

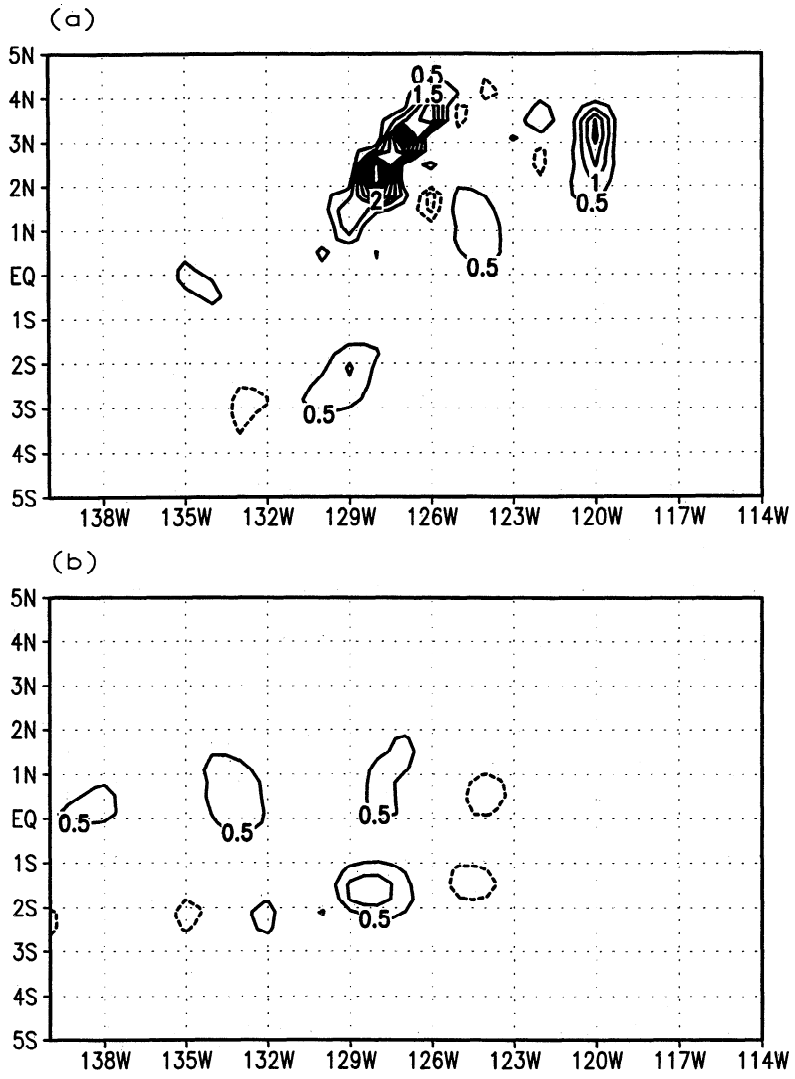

Figure 15. As in Figure 13 but at 95 m.

cific of the temperature field at the uppermost level of the model superimposed on the vertically averaged K_e (shaded area). The boxes delimit the areas for which we compute the volume budget of the energetics. It is important to note that the crest of the fully developed wave (wave 2) is distinguished by two separate K_e maxima which develop on the upstream and downstream sides of the crest. As in the atmospheric case, the most eastward K_e maximum (wave 1 in Figure 17) has a baroclinic nature. The K_e maximum located at 1°S between 123° and 126°W in Figure 17b develops through a barotropic process that we have shown happens at the surface (see Figure 13b). On the contrary, north of the equator, the K_e center located at 2°N between 126° and 128°W in Figure 17b develops both through eddy pressure flux convergence and through baroclinic conversion (compare Figures 13a and 15a). This process is very similar to what happens in the atmosphere in the downstream development of cyclone waves. In the oceanic case the vertical eddy fluxes are very important in the development of the waves. The previous energy analysis performed at different levels demonstrates that the K_e maxima of both waves 1 and 2 grow below the surface mainly through baroclinic conversion. Subsequently, vertical and horizontal eddy pressure fluxes transport energy upward and westward to trigger the secondary K_e maxima north and south of the equator that are seen in Figure 14a. The northern and southern surface K_e maxima then develop through baroclinic and barotropic conversions, respectively, which dominate the convergence of the pressure flux.

Since the waves are not stationary and have a westward propagation, the evolution of each wave, i.e., its life cycle, cannot be examined by computing the energetics for a given area or volume fixed in time. On the contrary, it is necessary to isolate a volume which identifies an individual eddy and calculate the volume budget of the eddy kinetic energy equation as the eddy is propagating westward. In particular, we examine the life cycles of two individual eddies identified as waves

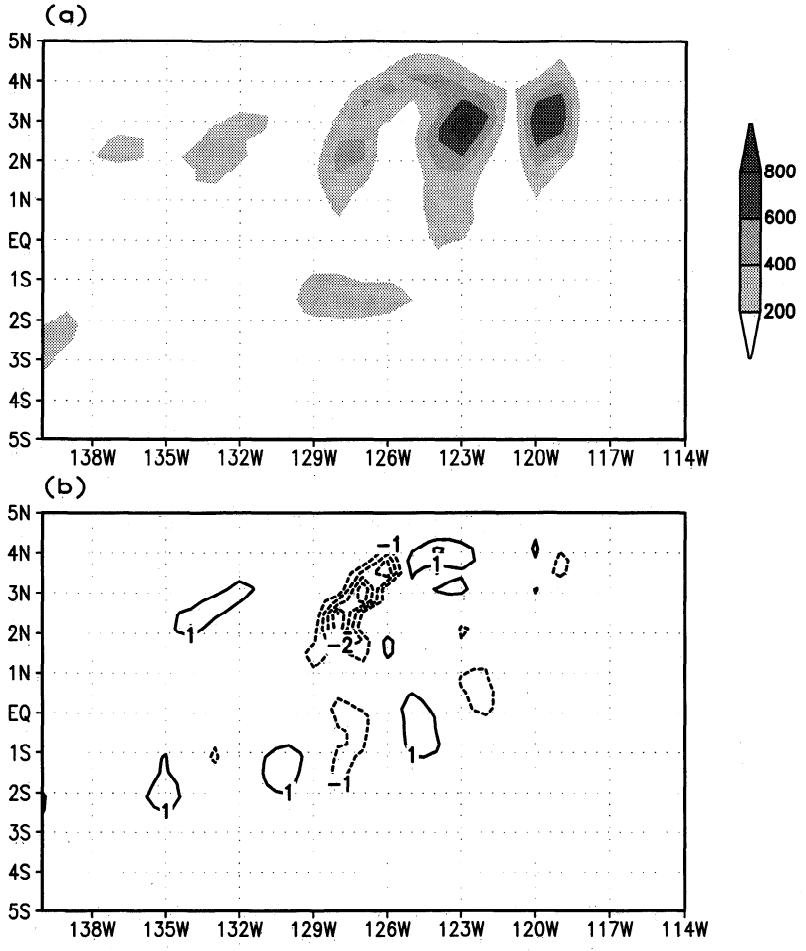

Figure 16. As in Figure 14 but at 95 m. Contour intervals are 200 x 10^{-3} cm^2/s^2 in Figure 16a and 1 x 10^{-3} cm^2/s^3 in Figure 16b.

1 and 2, shown in Figure 17 at two instants 6 days apart, during their westward propagation. The area which identifies each eddy is chosen so that it delimits the same volume at all times and is centered over one crest of the wave, extending over one wavelength. Since there are two different energetic processes that happen north and south of the equator, we decided to distinguish the northern part of the waves from the southern part. As far as the length of the life cycle is concerned, it is self-defined since it is determined by the growing and successive decaying phase of the individual eddy. The two eddies, waves 1 and 2, were tracked for 27 days during their westward propagation. Figures 18 and 19 show the evolution of the volume budget of the northern and southern part of each eddy during the growing and decaying phase. Quantities in Figures 18 and 19 are volume-averaged, where the volume is taken to be the area delimiting each eddy at each time step times the basin depth. We chose 27 days because 27 days represent approximately the period of the wave (see MP99). During one period both waves 1 and 2 move westward, covering one wavelength distance. In practice, after one period, wave 1 is located where wave 2 was 27 days before, and wave 2 is centered over the most westward crest of the wave, which is the one centered at 134°W in Figure 17a and identified by the two most westward K_e relative maxima. Westward of that longitude, the waves dissipate, and it is not even possible to identify an individual eddy. The two curves in Figure 18a represent the volume-averaged K_e of the northern part of the two eddies. Wave 1 is captured during its growing phase (increasing K_e curve), while wave 2 is decaying (decreasing K_e curve). In the volume-averaged energetics of both waves (Figures 18b and 18c) the largest positive contribution is from baroclinic conversion (solid circles), while the eddy pressure flux divergence (open squares) is always a sink. The other two curves in each plot represent the barotropic conversion (solid squares) and the K_e advection (diamonds), and they both are clearly negligible in the volume average. As in the atmospheric case at the entrance of a storm track [*Chang and Orlanski,* 1993, Figure 8a], eddy growth is due primarily to baroclinic conversion and eddy decay to the divergence of eddy pressure flux (see Figures 18b and 18c). In the energetic analysis that we have performed at each level, there is evidence of a region north of the equator where the eddy fluxes are convergent, but in the volume average, there is clear indication that the

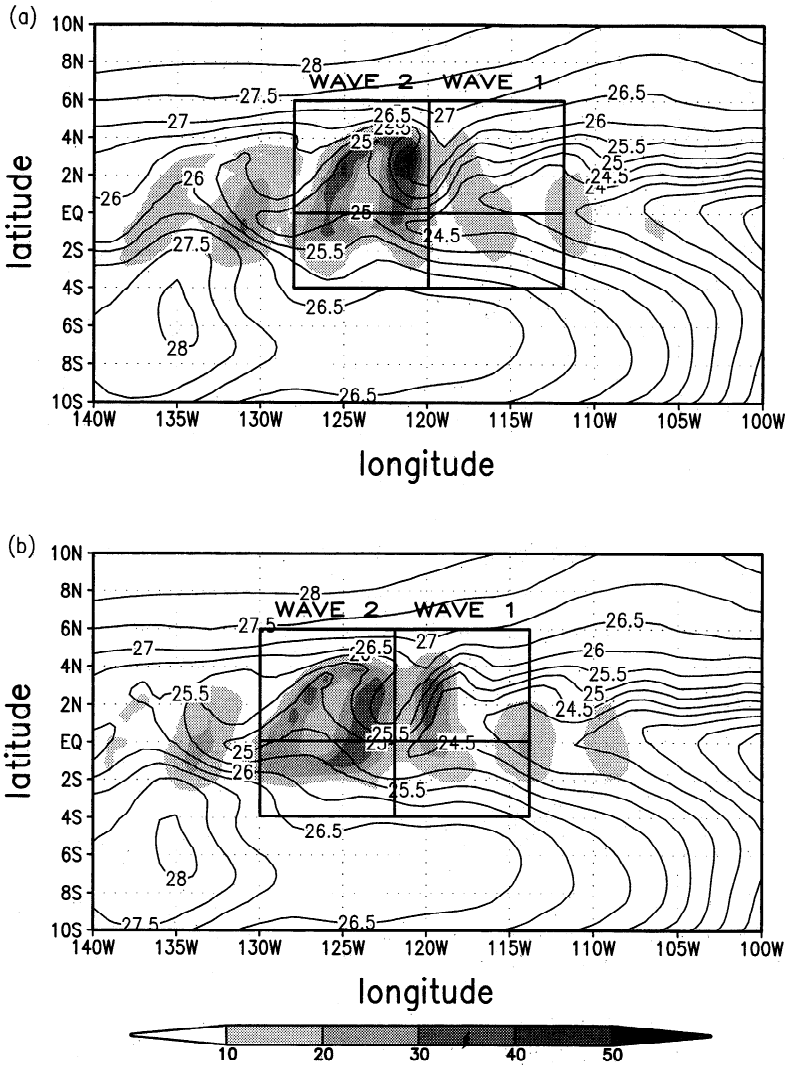

Figure 17. (a) Latitude-longitude snapshot at t=3 days of vertically averaged eddy kinetic energy (shaded; CI is 10 dyn/cm^3) and SST (contour; CI is 0.5°C). The boxes denote the areas for which the volume budgets shown in Figures 18 and 19 are computed. (b) As in Figure 17a but at t=9 days.

role of the eddy fluxes is mainly to transport energy away from the region north of the equator. As the time average analysis presented in section 4 has already suggested, the eddy pressure fluxes transport energy across the equator and trigger the growing phase of wave 1 south of the equator. This is nicely illustrated in Figure 19, which shows the evolution of the energetics of waves 1 and 2 south of the equator. Here both the growing and decaying phases of the waves are time lagged with respect to the correspondent phases of the waves north of the equator. In particular, wave 1 south of the equator starts to grow after its northern part (compare Figures 18a and 19a), and it grows as a consequence of the convergence of eddy pressure flux, which is the only significative source of energy south of the equator in the volume average (Figure 19b).

Therefore, in the oceanic case the eddies south of the equator evolve in a way similar to the atmospheric downstream eddy development in the middle of a storm track. In the atmosphere the eddy pressure fluxes transport energy downstream from an upstream K_e center, whereas in the ocean they transport energy from a northern K_e center mainly southward across the equator. The eddy fluxes trigger an unstable process marked by baroclinic conversion in the atmosphere and by barotropic conversions south of the equator in the ocean. In contrast to the atmospheric case in which the downstream eddies decay through divergence of eddy pressure fluxes [*Chang and Orlanski,* 1993, Figure 8b], the oceanic case exhibits southern eddies that weaken through barotropic decay (see Figure 13b). Note that these local dynamics are not revealed in the volume averaged quantities of Figures 18 and 19 because of the different roles played by the barotropic conversion term in different parts of the wave.

We have shown that TIWs in the Pacific Ocean are

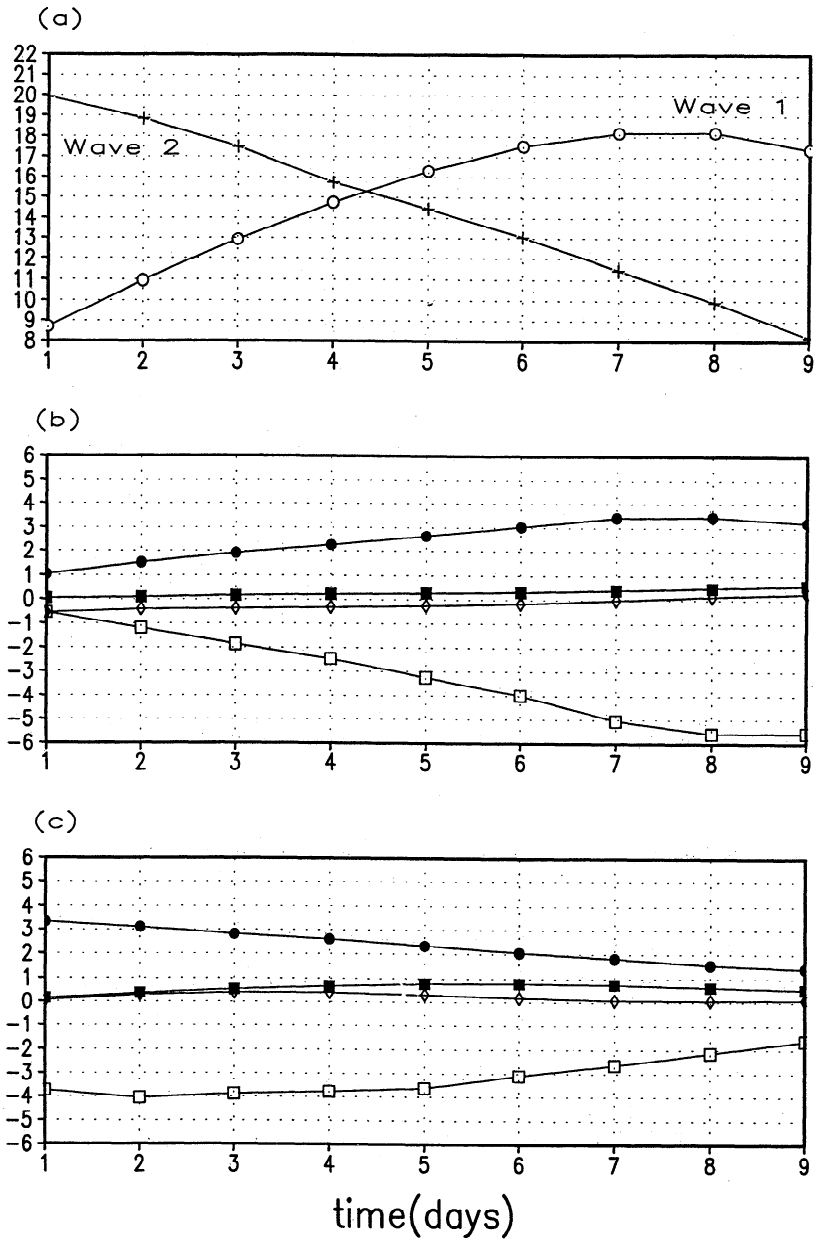

Figure 18. (a) Eddy kinetic energy (dyn/cm^3) of wave 1 (open circles) and wave 2 (crosses) north of the equator. (b) Baroclinic conversion (solid circles), eddy pressure flux divergence (open square), barotropic conversion (solid squares) and eddy kinetic energy advection (diamonds) for wave 1. (c) As in Figure 18b but for wave 2. In Figures 18b and 18c the unit is 10^{-5} cm^2/s^3.

a complex, mixed phenomenon characterized by local baroclinic instability north of the equator and eddy flux convergence south of the equator. As in the case of atmospheric baroclinic waves, the disturbances grow initially through baroclinic instability. Later in the life cycle, the convergence and divergence of eddy pressure fluxes play a fundamental role. In the atmospheric case the eddy pressure fluxes are the primary source of energy during the initial growth of a downstream eddy with baroclinic instability becoming important 2-3 days later. In practice, in the atmospheric case the eddy pressure fluxes trigger the growth of a second downstream baroclinic eddy, whereas in the ocean case they transport energy cross equatorial and downstream and trigger the growth of a barotropic and a baroclinic eddy south and north of the equator, respectively. This means that if we consider averaged quantities in the volume containing an eddy, the pressure flux divergence in the oceanic case is always negative north of the equator (because it works to partly balance the energy production due to instability processes) and is always positive south of the equator (where the fluxes trigger an equatorial barotropic mode that is part of the wave structure). In the atmospheric case the pressure flux diver-

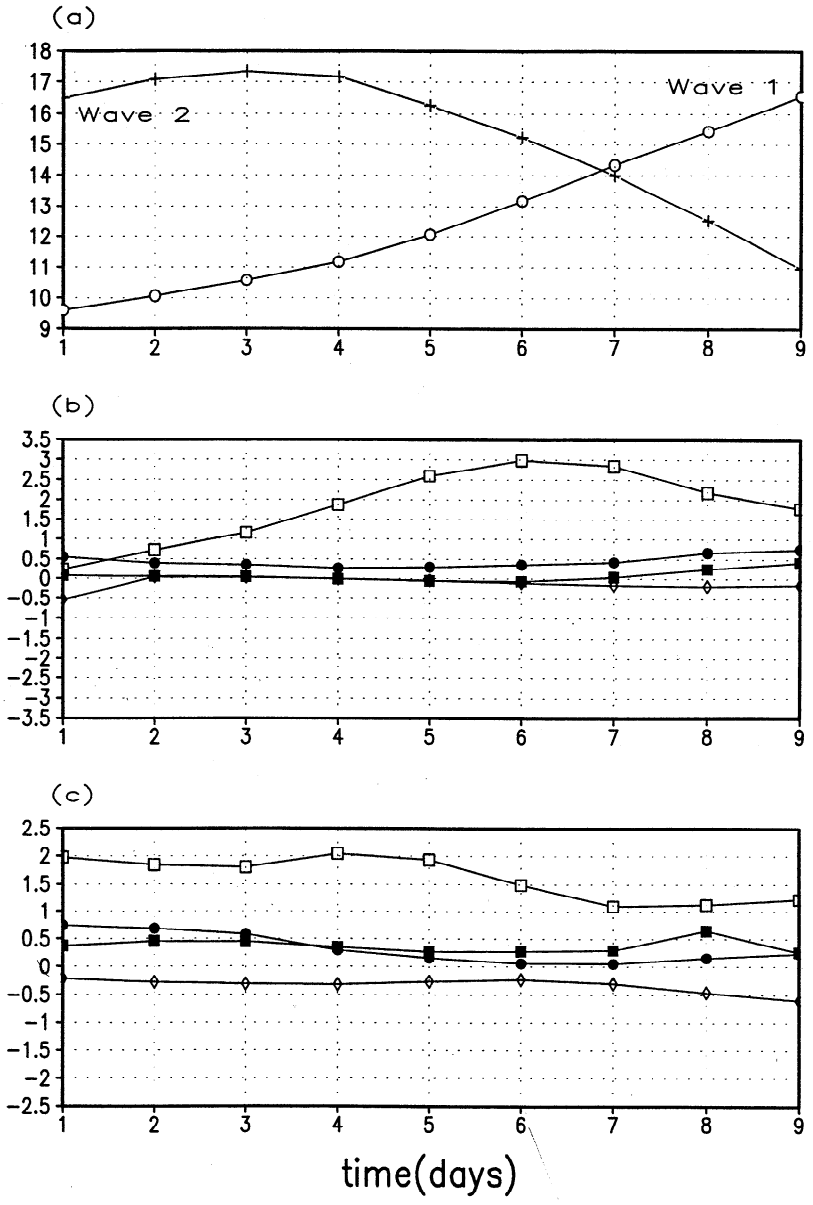

Figure 19. As in Figure 18 but for waves 1 and 2 south of the equator.

gence represents an energy sink (it is negative) for the eddies at the entrance of the storm track and an energy source (it is positive) during the initial growth phase of a downstream eddy [*Chang and Orlanski,* 1993]. In the oceanic case we have shown that if we do not take the volume average and look at the different terms of (9) locally, the horizontal and vertical pressure fluxes are seen to play an important role in the evolution and propagation of TIWs at all latitudes.

6. Summary and Conclusions

By studying the energetics of the TIWs that arose in the numerical simulation of the Pacific Ocean (MP99) we have shown the key mechanisms that generate and propagate these waves. We use a technique that is based on an eddy kinetic energy budget that defines the eddies as deviations from the time mean flow. A similar formulation for the atmosphere has been recently applied to explain the downstream development in atmospheric storm tracks [*Orlanski and Katzfey,* 1991; *Chang and Orlanski,* 1993].

The instabilities generated in the eastern Pacific consist of two components phase locked to each other. One component develops between 2°S and the equator, and the other develops between 2° and 4°N. Diagnostics of the local energy sources and sinks in the TIWs show that these waves are primarily generated through baroclinic instability located from 2° to 6°N with barotropic instability playing the dominant role closer to the equator. We have shown that the northern temperature front becomes unstable in the eastern Pacific, while the

southern front is weakly unstable in the central Pacific. The mean flow is also unstable both in the eastern and central Pacific through barotropic shear between the EUC and the SEC. Our study shows that the shear between the SEC and the NECC is never barotropically unstable in our simulations. In the eastern Pacific the barotropic and baroclinic instabilities explain the two-peak structure of the TIWs. Despite some data suggesting two different modes decoupled in latitude [*Flament et al.*, 1996] our study indicates that the two modes are coupled and phase locked at all depths.

In the central Pacific, because of the deepening of the EUC and the presence of a southern branch of the SEC, the mean flow is barotropically unstable at deeper levels (with respect to the eastern Pacific) and on both sides of the EUC. This complicated mean state gives rise to the complex structure of the unstable oscillations at these longitudes. However, as in the eastern Pacific, the oscillations grow both from barotropic and baroclinic conversions.

The time mean energy budget indicates that the combined barotropic $(-\overline{u'v'}(\partial U/\partial y))$ and baroclinic $(-g\overline{\rho'w'})$ conversions explain the energy distribution at and north of the equator, respectively. The other deformation work terms and the advection terms are negligible in a time mean sense in these regions. The eddy pressure fluxes transport part of the K_e poleward of the unstable region and, in particular, explain the presence of eddy kinetic energy south of the equator in the eastern Pacific.

In summary, the processes that control the life cycle of TIWs in the Pacific Ocean and their westward propagation show some characteristics similar to the atmospheric development of a cyclone wave. We demonstrated that both the growing and the decaying phases of the eddies are controlled by baroclinic instability and by the divergence of eddy pressure fluxes north of the equator. The baroclinic conversion represents the only important source of energy if the energetics of each eddy are averaged in a volume containing the part of the eddy which develop north of the equator. The divergence of eddy pressure fluxes is the main sink of energy and partly balances the baroclinic conversion at each step of the life time of the waves. The barotropic conversion, in the volume average sense, is negligible. On the contrary, both the growing and decaying phases of the southern (south of the equator) part of the eddies are determined by the convergence of the eddy pressure fluxes. In particular, these fluxes trigger the growth of a southern eddy which grows and decays through barotropic conversion. However, the barotropic conversion is negligible in the volume average calculated south of the equator because of the different roles played by the barotropic conversion in different parts of the waves. The baroclinic conversion, in the volume average sense, is also negligible south of the equator. This mechanism is similar to the development of cyclone waves in the atmosphere [*Chang and Orlanski*, 1993] where the initial source of energy at the entrance of a storm track is baroclinic conversion while in the middle of the storm track a downstream eddy grows through the convergence of geopotential flux from a decaying upstream eddy; baroclinic conversions come into play only after 2-3 days. Therefore we can conclude that both the atmospheric eddies at the entrance of a storm track and the northern component of TIWs have a baroclinic nature. Also the development of the southern eddies in the oceanic case is similar to the downstream development of atmospheric eddies in the center of a storm track. In both cases the eddy pressure fluxes radiate energy away from the initial baroclinic centers. In the atmospheric case the pressure fluxes transport energy downstream and trigger another baroclinic eddy, while in the oceanic case they transport energy southward and trigger the barotropic component of TIWs.

Finally, our results show that the primary source of energy of the TIWs is baroclinic and that the waves are initially generated below the surface in the mixed layer north of the equator. The horizontal and vertical eddy pressure fluxes radiate the energy in the domain, and a subsequent barotropic instability occurs close to the surface at the equator.

Acknowledgments. We would like to thank I. Orlanski and K. Bryan for their helpful discussions and advice. This work was supported by the Department of Commerce/NOAA under grant NA56GP0026. One of the authors (SM) was partially supported by a NASA Global Change Fellowship NGT-30288. Another author (AB) was supported by a UCAR Postdoctoral Fellowship. We also thank two anonymous reviewers for their helpful comments.

References

Chang, E.K.M., and I. Orlanski, On the dynamics of a storm track, *J. Atmos. Sci., 50*, 999-1015, 1993.

Cox, M.D., Generation and propagation of 30-day waves in a numerical model of the Pacific, *J. Phys. Oceanogr., 10*, 1168-1186, 1980.

Flament, P., S. Kennan, R. Knox, P. Niiler, and R. Bernstein, The three-dimensional structure of an upper ocean vortex in the tropical Pacific, *Nature, 383*, 610-613, 1996.

Hansen, D.V., and C.A. Paul, Genesis and effects of long waves in the equatorial Pacific, *J. Geophys. Res., 89*, 10,431-10,440, 1984.

Hayashi, Y.Y., and W.R. Young, Stable and unstable shear modes of rotating parallel flows in shallow water, *J. Fluid Mech., 184*, 477-504, 1987.

Kuo, H.L., Dynamic instability of two-dimensional nondivergent flow in a barotropic atmosphere, *J. Meteorol., 6*, 105-122, 1949.

Legeckis, R., Long waves in the eastern equatorial Pacific Ocean: A view from a geostationary satellite, *Science, 197*, 1179-1181, 1977.

Luther, D.S., and E.S. Johnson, Eddy energetics in the upper equatorial Pacific during the Hawaii-to-Tahiti Shuttle Experiment, *J. Phys. Oceanogr., 20*, 913-944, 1990.

Marinone, S.G., and P. Ripa, Energetics of the instability of a depth-independent equatorial jet, *Geophys. Astrophys. Fluid Dyn., 30*, 105-130, 1984.

Masina, S., Tropical instability waves in the Pacific Ocean,

Ph.D. thesis, 242 pp., Princeton Univ., Princeton, N. J., 1996.

Masina, S., and S.G.H. Philander, An analysis of tropical instability waves in a numerical model of the Pacific Ocean, 1, Spatial variability of the waves, *J. Geophys. Res.*, this issue.

McCreary, J.P., Jr, and Z. Yu, Equatorial dynamics in a $2\frac{1}{2}$-layer model, *Prog. Oceanogr., 29*, 61-132, 1992.

McIntyre, M.E., An introduction to the generalized lagrangian-mean description of wave, mean-flow interaction, *Pure Appl. Geophys., 118*, 152-176, 1980.

McPhaden, M.J., Monthly period oscillations in the Pacific North Equatorial Countercurrent, *J. Geophys. Res., 101*, 6337-6359, 1996.

Orlanski, I., and J. Katzfey, The life cycle of a cyclone wave in the Southern Hemisphere, 1, Eddy energy budget, *J. Atmos. Sci., 48*, 1972-1998, 1991.

Peixoto, J.P., and A.H. Oort, *Physics of Climate,* 520pp., Am. Inst. of Phys. College Park, Md., 1992.

Philander, S.G.H., Instabilities of zonal equatorial currents, *J. Geophys. Res., 81*, 3725-3735, 1976.

Philander, S.G.H., Instabilities of zonal equatorial currents, 2, *J. Geophys. Res., 83*, 3679-3682, 1978.

Plumb, R.A., A new look at the energy cycle, *J. Atmos. Sci., 40*, 1669-1688, 1983.

Proehl, J.A., Linear stability of equatorial flows, *J. Phys. Oceanogr., 26*, 601-621, 1996.

Qiao, L., and R.H. Weisberg, Tropical instability wave kinematics: Observations from the Tropical Instability Wave Experiment, *J. Geophys. Res., 100*, 8677-8693, 1995.

Qiao, L., and R.H. Weisberg, Tropical instability wave energetics: Observations from the Tropical Instability Wave Experiment, *J. Phys. Oceanogr., 28*, 345-360, 1998.

Schopf, P.S., Shallow baroclinic instability in the tropical oceans, in *Recent Progress in Equatorial Oceanography*, edited by J.P. McCreary Jr., D.W. Moore, and J.M. Witte, pp. 189-195, Nova University Press, Ft. Lauderdale, FL, 1981.

Semtner, A.J., Jr, and W.R. Holland, Numerical simulation of equatorial ocean circulation, 1, A basic case in turbulent equilibrium, *J. Phys. Oceanogr., 10*, 667-693, 1980.

Weisberg, R.H., Equatorial Waves during GATE and their relation to the mean zonal circulation, *Deep Sea Res., Part A, 26*, suppl. 2, 179-198, 1979.

Wilson, D., and A. Leetmaa, Acoustic Doppler current profiling in the equatorial Pacific in 1984, *J. Geophys. Res., 93*, 13947-13966, 1988.

Yu, Z., J.P. McCreary Jr., and J.A. Proehl, Meridional asymmetry and energetics of tropical instability waves, *J. Phys. Oceanogr., 25*, 2997-3007, 1995.

A.B.G. Bush, Department of Earth and Atmospheric Sciences, University of Alberta, Edmonton, Alberta, Canada T6G 2E3. (andrew.bush@ualberta.ca)

S. Masina, ISAO, CNR, Via Gobetti, 101, 40129 Bologna, Italy. (s.masina@isao.bo.cnr.it)

S.G.H. Philander, Atmospheric and Oceanic Sciences, Princeton University, Princeton, N.J., 08544. (gphlder@splash.Princeton.EDU)

(Received November 12, 1997; revised April 12, 1999; accepted July 28, 1999.)